International Journal of Pharmaceutics 690 (2026) 126514

Contents lists available at ScienceDirect

International Journal of Pharmaceutics

journal homepage: www.elsevier.com/locate/ijpharm

Quality-by-design-steered development of luliconazole-loaded ultra-deformable ethosomes for topical delivery: improved dermatokinetics and antifungal activity

Akanksha Mahajan [a,b], Gajanand Sharma [a], Sarah R. Dennison [c], Kamalinder K. Singh [b,c,*], Bhupinder Singh [a,**], Om Prakash Katare [a,**]

[a] University Institute of Pharmaceutical Sciences, Panjab University, Chandigarh 160 014, India
[b] School of Pharmacy and Biomedical Sciences, University of Lancashire, Preston PR1 2HE, United Kingdom
[c] Biomedical Evidence Based Transdisciplinary (BEST) Health Research Institute, University of Lancashire, Preston PR1 2HE, United Kingdom

ARTICLE INFO

Keywords:
Luliconazole
Ultra-deformable ethosomes
Trichophyton rubrum
Time-kill kinetics
HaCaT keratinocytes
Box-Behnken design
Ex vivo permeation
Retention studies

ABSTRACT

This work reports the first systematic formulation strategy guided by Quality-by-Design (QbD) principles to create an ultra-deformable ethosomes (UDEs) based nanocarrier for luliconazole (LCZ). The approach addresses the long-standing barriers of poor solubility, limited skin penetration, and rapid drug clearance in dermatophytosis therapy. A Box-Behnken design identified the optimal composition, including phospholipid (PL 90G), Span® 20, and ethanol: propylene glycol, yielding highly elastic nanosized vesicles (particle size 196.97 ± 1.57 nm; polydispersity index 0.158 ± 0.03) with exceptional percent drug entrapment (91.0%) and sustained release (62% over 12 h). Incorporation into a Carbopol 980 gel conferred favourable shear-thinning behaviour, enhanced spreadability, and superior texture as compared to a marketed 1% LCZ cream (MKT-LF). *Ex vivo* permeation across rat skin demonstrated a 2.4-fold higher flux and 11.3-fold greater cutaneous deposition than MKT-LF, attributed to synergistic vesicle deformability and ethanol-induced fluidization of stratum corneum. LCZ-UDEs demonstrated deep epidermal penetration of intact fluorescently labelled vesicles. Dermatokinetic profiling revealed a 3.4-fold increase in epidermal $AUC_{0\text{-}12}$, prolonged half-life, and delayed T_{max}, indicating enhanced skin retention. Antifungal assays demonstrated a two-fold reduction in MIC, and rapid fungicidal kinetics against *Trichophyton rubrum* compared with LCZ solution and MKT-LF. Biocompatibility studies validated >90% HaCaT cell viability, no haemolysis, and absence of dermal irritation. Sustained intradermal LCZ levels minimized sub-therapeutic exposure that drives fungal resistance. By uniting nanoscale vesicle engineering, ethanol-enhanced skin permeation, and QbD-optimized composition, this study delivers a stable, safe, and efficacious topical nanoplatform with potential to transform dermatophytosis management and mitigate antifungal resistance.

1. Introduction

Dermatophytosis affects approximately 25% of the world's population, with *Trichophyton rubrum* leading tinea pedis, corporis, cruris cases (Dellièree et al., 2024). Indian prevalence reaches 37–78%, driven by humid climate, overcrowding, poor hygiene, diabetes, and immunosuppression (Kumar et al., 2023). Although the antifungal agents, both topical (e.g., clotrimazole, ketoconazole, terbinafine) and systemic (e.g., itraconazole, terbinafine), are commonly prescribed, they exhibit poor skin penetration, rapid drug clearance, and systemic toxicity, promoting relapse and resistance (Ahmed et al., 2025). Antifungal resistance in *Trichophyton* species often results from incomplete fungal eradication and repeated sub-therapeutic exposure due to inadequate epidermal drug retention. (Hussain et al., 2023).

Luliconazole (LCZ), an imidazole antifungal FDA-approved in 2013, blocks lanosterol 14α-demethylase to disrupt ergosterol synthesis and kill fungi (Nosratabadi et al., 2024). Despite high lipophilicity (log P 4.07), LCZ is almost water-insoluble (0.0034 ± 0.000067 mg/mL),

* Corresponding author at: School of Pharmacy and Biomedical Sciences, University of Lancashire, Preston PR1 2HE, United Kingdom.
** Corresponding authors at: University Insitute of Pharmaceutical Sciences, Panjab University, Chandigarh 160014, India.
E-mail addresses: ksingh1@lancashire.ac.uk (K.K. Singh), bsbhoop@gmail.com (B. Singh), drkatare@yahoo.com (O.P. Katare).

https://doi.org/10.1016/j.ijpharm.2025.126514
Received 5 October 2025; Received in revised form 30 November 2025; Accepted 16 December 2025
Available online 17 December 2025

penetrates stratum corneum poorly, clears rapidly from skin, and degrades under light or oxygen (dos Santos Porto et al., 2022). LCZ is classified under the Biopharmaceutics Classification System (BCS) Class II, exhibiting low aqueous solubility but high permeability, which contributes to its dissolution-limited absorption profile and challenges in topical bioavailability. Conventional 1% LCZ creams and gels often fail to reach deeper skin layers, leaving fungal reservoirs untreated and increasing relapse risk. Moreover, active fungal efflux mechanisms and limited drug retention at the infection site diminish its therapeutic efficacy (Kaur et al., 2024). Further, these formidable challenges demand advanced topical delivery strategies capable of enhancing skin penetration, improving drug localization, and providing sustained drug release.

To overcome the aforementioned formulation challenges, nanocarrier-based drug delivery systems offer a promising solution to enhance topical bioavailability and skin targeting by improving solubility, protecting unstable drugs, increasing dermal permeability, and facilitating site-specific deposition. Lipid-based nanocarriers, including liposomes (Kaur et al., 2020), ethosomes (Lin et al., 2022), solid lipid nanoparticles (SLNs) (Kaur et al., 2024; Saini et al., 2022), niosomes (Garg et al., 2021), nanostructured lipid carriers (NLCs) (Ebrahimi Barogh et al., 2025), and nanoemulsions (Alhakamy et al., 2021; Vats and Nigam, 2023), have been widely employed as topical drug delivery systems (Haider et al., 2020; Nene et al., 2021; Pinilla et al., 2021). Other systems, including polymeric nanoparticles, metal nanoparticles, and nanocrystals, have also shown distinct potential for enhancing cutaneous drug deposition (Madawi et al., 2023; Nosratabadi et al., 2024). However, such systems suffer from critical limitations. The liposomes exhibit poor penetration due to rigid bilayers, the SLNs often encounter drug expulsion and instability (Prajapati et al., 2025), the NLCs and nanoemulsions can aggregate or cause burst release (Mall et al., 2024), while the conventional ethosomes can suffer from vesicular leakage, oxidative degradation, limited elasticity, and skin irritation.

Nanoformulations like ultra-deformable ethosomes (UDEs) offer critical advantages for topical drug delivery due to their nanoscale size (typically $<$ 300 nm) and exceptional elasticity (Seenivasan et al., 2025). These phospholipid vesicles, enriched with high ethanol content and an edge activator such as Span® 20, are designed to traverse the intact stratum corneum via narrow intercellular pathways, thus enabling enhanced intercellular penetration and deeper deposition of active agents within the epidermis and dermis (Chauhan et al., 2025). The small size of UDEs facilitates intimate contact with the skin surface, while their deformability enhances permeability and promotes effective skin localization of the drug, critical for treating chronic infections like dermatophytosis (Gopi and Balakrishnan, 2024). Moreover, the nanoscale size and ultra-deformable bilayer architecture of UDEs allow them to maintain prolonged and intimate contact with the skin surface, forming a hydration-driven diffusion reservoir that supports sustained drug delivery to superficial layers. The high deformability enables these vesicles to navigate through narrow intercellular lipid channels of the stratum corneum without structural disruption, promoting deep epidermal penetration where fungal colonies typically persist. This combination of prolonged skin adhesion and adaptive deformation not only enhances localized LCZ deposition but also contributes to improved therapeutic efficacy against chronic dermatophytic infections (Noreen et al., 2023; Peram et al., 2025; Souto et al., 2021; Zhan et al., 2024). Furthermore, sustained intradermal delivery via UDEs can maintain fungicidal levels within infected strata, reducing relapse frequency and minimizing the emergence of resistant strains (Hussain et al., 2023).

Ethanol plays a dual role by fluidizing both ethosomal and skin lipids, thereby enhancing vesicle flexibility and improving skin permeation, while also contributing to formulation stability (Natsheh and Touitou, 2020). Propylene glycol (PG) further enhances drug solubilization and acts synergistically with ethanol to improve skin permeation without compromising vesicle integrity (Manconi et al., 2019). The inclusion of Span® 20 significantly increases membrane flexibility, thus reducing the risk of vesicle rupture and drug leakage (Bnyan et al., 2018). Menthol provides a reversible keratolytic effect, temporarily disrupting the lipid packing of the stratum corneum to facilitate diffusion and retention (Lan et al., 2016). Taken together, this innovative delivery platform can potentially overcome the principal shortcomings of the conventional LCZ formulations by significantly enhancing skin permeability, ensuring sustained drug localization at the infection site. It further minimizes systemic exposure while providing superior formulation stability. It is noteworthy that while UDEs facilitate penetration into the viable epidermis and upper dermis, their nanoscale vesicles do not traverse into systemic circulation. This controlled depth of penetration ensures effective delivery to infection sites while preventing systemic absorption, thereby maintaining an optimal balance between localized efficacy and safety. This structural design, combining ethanol-mediated bilayer fluidization with the viscosity of the gel matrix, enables UDEs to achieve deep epidermal permeation while sustaining local retention for prolonged therapeutic action. Moreover, by sustaining high localized LCZ concentrations and preventing sub-therapeutic diffusion into deeper tissues, the optimized UDE design can reduce fungal persistence and the potential development of antifungal resistance (Dellièree et al., 2024). To address these challenges in a structured way, the Quality by Design (QbD) framework offers a science-driven, regulatory-aligned approach to identify and control critical variables, ensuring that nanocarrier systems are optimized, reproducible, and clinically translatable.

Anchored in QbD principles, this study develops an UDEs system for LCZ. The optimized platform harnesses a strategically balanced composition of ethanol, propylene glycol, Span®20, and menthol to achieve promising vesicle elasticity, nanoscale precision, and formulation stability, while overcoming the penetration, retention, and degradation barriers in LCZ therapy. Although several nanocarrier platforms, such as transferosomes, nanosponges, nanocrystals, and nanoemulgels, have already been reported for LCZ delivery (Kapileshwari et al., 2020; Nidbane et al., 2025), these systems generally optimized a limited number of formulation variables and evaluated narrower endpoints, primarily focusing on physicochemical characterization or basic antifungal testing, without adopting a systematic QbD framework or performing integrated dermatokinetic and mechanistic analyses. In contrast, the present investigation introduces a QbD-steered ultra-deformable ethosomal platform that uniquely integrates edge activation (Span® 20) with ethanol-propylene glycol modulation to achieve exceptional deformability, high drug entrapment, and superior formulation stability. The study further distinguishes itself by employing a complete DoE pipeline (Ishikawa/FMEA → Taguchi screening → Box-Behnken optimization) and by conducting a comprehensive evaluation encompassing dermatokinetic profiling, intact-vesicle visualization by confocal microscopy, and standardized fungicidal kinetics benchmarking against a marketed 1% LCZ cream. This integrative design and validation framework differentiates the present formulation from the previously reported LCZ nanocarriers and underscores its novelty and clinical promise.

2. Materials and methods

2.1. Materials

Luliconazole (LCZ, ≥98.5% purity) was kindly provided as a complimentary sample by Psyco Remedies Ltd. and BDH Industries, Mumbai. Phospholipon 90G (PL 90 G, ≥90% phosphatidylcholine content) was obtained from Lipoid GmbH, Nattermannallee, Germany. Additional excipients, including Span® 20 (sorbitan monolaurate, ≥99.2% purity) from S.D. Fine-Chem. Ltd. (Mumbai, India), ethanol (≥99.9% purity) and propylene glycol (PG, ≥99.5% purity) from Loba Chemie (Mumbai, India), butylated hydroxytoluene (BHT, ≥99.0% purity) from Fisher Scientific (India) and Sabouraud dextrose agar (SDA) from Fisher Scientific UK, were used as received without further purification.

Throughout the experimental work, HPLC-grade water (conductivity < 1.0 μS/cm) served as the solvent. A commercially available LCZ formulation was purchased from a local retail pharmacy for comparison.

2.2. QbD-based development and optimization of LCZ-UDEs

The Quality Target Product Profile (QTPP) was defined to ensure the safety, efficacy, and stability of LCZ-UDEs, enabling the systematic identification of critical quality attributes (CQAs), as shown in Table S1 (vesicle size, percent drug release, and percent drug entrapment, i.e., PDE), by aligning product attributes with measurable quality criteria. Although zeta potential is an important indicator of colloidal stability, it was not designated as a CQA in this study because preliminary screening confirmed that all trial UDEs dispersions exhibited ζ-potential values greater than −20 mV, indicating adequate inherent stability. Potential formulation and process risks impacting CQAs were explored using an Ishikawa diagram and Failure Mode and Effects Analysis (FMEA). Material attributes (MAs), including lipid type/concentration, edge activator type/concentration, and ethanol percentage, and process parameters (PPs) such as stirring speed, hydration, and ultracentrifugation, were scored for severity, occurrence, and detectability to calculate risk priority number (RPN) values, classifying them into low, medium, or high-risk factors as presented in Table S2. A Taguchi orthogonal array was used for preliminary screening, testing seven MAs/PPs at two levels across eight runs. Key variables affecting CQAs (vesicle size, PDE) included phospholipid type/concentration, edge activator concentration/type, ethanol%, PG concentration, and stirring conditions. A Box-Behnken design (BBD) evaluated three critical material attributes (CMAs), *viz.,* phospholipid concentration (X_1), edge activator concentration (X_2), and ethanol: PG ratio (X_3), across 15 runs (Table S3). Four centre-point replicates ensured reproducibility, with responses analyzed for vesicle size, percent drug release, and PDE (Houacine et al., 2020; Pant et al., 2024a).

2.3. QbD-guided optimization: Analysis and validation of data

LCZ-UDEs were optimized under a QbD framework by modeling vesicle size (nm), drug release (%), and PDE via multiple linear regression analysis using quadratic polynomials based on significant coefficients, with adequacy supported by p-values, coefficient of variation (CV), coefficient of determination (r^2) and predicted residual sum of squares. Response surfaces and contour plots depicted factor-response relationships, and numerical and graphical methods, with overlay plots, defined the design space and optimal region. Predictive performance was confirmed using checkpoint formulations within the design space by comparing experimental versus model-predicted responses and calculating relative errors (Pant et al., 2024b).

2.4. Preparation method of ultra-deformable ethosomes (UDEs)

Excipients (PL90G, ethanol, Span® 20, menthol, PG) were chosen from solubility data, in-house findings, and literature support (Natsheh and Touitou, 2020). UDEs were produced by modified ethanol injection with high-shear mixing: LCZ, PL90G, Span® 20, menthol, and BHT were dissolved in ethanol at 40 °C under 100 rpm to form the organic phase; PG in water was prepared similarly as the aqueous phase (Sharma et al., 2023). The aqueous phase was slowly added to the ethanolic phase under constant stirring, followed by 30 min mixing to yield a homogeneous suspension of LCZ-loaded ultra-deformable vesicles.

The resulting LCZ-UDEs was stored under refrigerated conditions (2–8 °C) in airtight vials for further characterization and stability studies. Fig. S1 provides a schematic overview of the preparation process.

2.5. Measurement of particle size, zeta potential, and polydispersity index (PDI)

Particle size and PDI were determined by dynamic light scattering (Nano ZS90, Malvern) at 25 °C after 1:100 dilution with de-ionized water. The values are mean of three runs. Zeta potential was measured on the undiluted dispersion (n = 3) at 25 °C under a 23.2 V/cm field (Sharma et al., 2022).

2.6. Percent drug entrapment (PDE), drug payload (%DPL), and vesicle quantification

LCZ-UDEs were ultracentrifuged (40,000 rpm, 1 h, 4 °C) to separate free drug; the pellet was washed, digested in chloroform: methanol (2:1 v/v), and quantified by HPLC against blank UDEs to correct excipient interference, with PDE and %DPL computed from standard equations (Erkut et al., 2025; Panthi and Nepal, 2022). A tenfold–diluted sample was loaded on a Neubauer hemocytometer, vesicles counted across 80 small squares by optical microscopy, and concentration calculated via the designated counting equation (Mehmood et al., 2024).

2.7. Evaluation of vesicle deformability

The deformability index (%) of LCZ-UDEs was evaluated using a vesicle extrusion method with an extruder system (Eastern Scientific Inc., USA), where the vesicular dispersion was forced through a polycarbonate membrane with a pore size of 50 nm. The vesicle size was measured both before and after extrusion using a Malvern Zetasizer Nano Series (Malvern Instruments Ltd., UK). The deformability index (%) was determined using Eq. (1), where PE and PA represent the mean vesicle size prior to and after the extrusion process (n = 3), respectively (Molinaro et al., 2019).

$$\text{Deformability index } (\%) = \frac{(PE - PA)}{PA} \times 100 \quad (1)$$

2.8. Thermal and spectroscopic analysis

Differential Scanning Calorimetry (DSC) (Q20, PerkinElmer) assessed thermal behavior of LCZ, excipients, and LCZ-UDEs using 2–5 mg samples sealed in aluminum pans, heated from 20-300°C at 10 °C/min under nitrogen purge (22 mL/min), with thermograms processed via StepScan to infer physical state and component interactions (Helal et al., 2025). Fourier transform infrared spectroscopy (FT-IR) (Spectrum Two, PerkinElmer) evaluated drug-excipient and formulation interactions at 25°C over 4000–400 cm^{-1} using KBr pellets (2:98 w/w, sample: KBr) in transmission mode to confirm functional groups and potential compatibility (Kaur et al., 2017).

2.9. Microscopic characterization by Field emission scanning electron micrscopy (FE-SEM)

LCZ-UDEs morphology was examined by FE-SEM (JEOL), wherein air-dried samples were mounted on aluminum stubs, sputter-coated with gold, and imaged at 15 kV to visualize vesicle shape, surface topography, and structural integrity (Thakur et al., 2019).

2.10. Incorporation of LCZ-UDEs into Carbopol 980 gel

Carbopol 980 gel (0.7% w/v) was prepared by dispersing the polymer in minimal water at 400 rpm and hydrating for 24 h to obtain a smooth base. 20 mL of optimized LCZ-UDEs (200 mg LCZ) was then gently blended into the base, and pH was adjusted to around 6.5–7.0 with dropwise triethanolamine to yield a uniform LCZ-UDEs gel. Thereafter, the homogeneity of the LCZ-UDEs gel, was evaluated visually by confirming the absence of lumps and phase separation, and also

evaluated for flow behaviour (rheology and texture analysis) to ensure the uniform consistency of the prepared gel.

2.11. Evaluation of the LCZ-UDEs gel formulation

2.11.1. pH measurement and physical stability assessment

The gel pH was measured at ambient temperature using a calibrated digital pH meter standardized with buffer solutions, with triplicate readings reported as the mean. Visual and physical stability were monitored for 4 weeks at room temperature, recording changes in color, odour, crystal formation, gel texture, liquefaction, and phase separation (Kumar et al., 2019).

2.11.2. Flow behavior analysis and texture analysis

Flow curves for LCZ-UDEs gel and marketed 1% LCZ cream (MKT-LF, Lulifin®) were recorded on a cone-and-plate rheometer at 30 ± 0.5 °C over 0–100 s^{-1}, and τ-γ data were fitted to the Herschel-Bulkley model ($\tau = \tau_0 + k\gamma^n$) to extract yield stress (τ_0), consistency (k), and flow index (n) describing shear-thinning or thickening behavior (Dandagi et al., 2020). Mechanical performance (firmness, consistency, adhesiveness, extrusion force) of the LCZ-UDEs gel and MKT-LF cream was quantified using a Texture Analyzer™ (Stable Micro Systems Ltd., UK) equipped with a TTC spreadability rig and a 5 kg load cell. Measurements were conducted at 25 ± 1 °C with a probe travel distance of 10 mm and test speed of 2 mm/s.

The parameters were calculated from the force–time curve to derive firmness (maximum force), consistency (positive area), adhesiveness (negative area), and work of cohesion (return area) (Al-Smadi et al., 2025; Yılmaz Usta et al., 2024).

2.11.3. Evaluation of formulation stability

Stability of LCZ-UDEs gel was assessed as per ICH Q1A(R2) for 6 months under refrigerated (5 ± 3 °C) and accelerated (40 ± 2 °C/75% ± 5% RH) conditions, with initial assay recorded before storage. Formulations in sealed collapsible tubes were sampled at 1, 3 and 6 months to evaluate appearance (color, odor, texture/grittiness), phase separation, pH, and drug content by validated HPLC method with detection at 296 nm, performed in triplicate for reliability (Chalikwar et al., 2025).

2.11.4. In vitro release and kinetic studies

The in vitro release behavior of LCZ-UDEs and LCZ-UDEs gel formulations was evaluated using the dialysis bag diffusion method. A weighed amount of each formulation (equivalent to 0.5g) was placed into a pre-activated dialysis membrane (molecular-weight cut-off 10–12 kDa; HiMedia, India). The dialysis sacs were immersed in 30 mL of release medium, consisting of phosphate-buffered saline (PBS, pH 7.4) and ethanol in an 80:20 (v/v) ratio, selected to maintain sink conditions for the poorly water-soluble LCZ. The assembly was maintained at 32 ± 0.5 °C under continuous magnetic stirring (100 rpm) to simulate the skin surface environment (Kaur et al., 2020).

At predetermined intervals over the period of 48 h, 1 mL aliquots were withdrawn from the receptor phase and replaced immediately with an equal volume of fresh medium to preserve constant sink conditions. The samples were filtered through 0.22 μm membranes and analysed by the validated HPLC method to quantify LCZ concentration. Cumulative drug release was calculated, and the resulting data were fitted to vital kinetic models, *viz.*, zero-order, first-order, Higuchi, Korsmeyer-Peppas, and Hixson-Crowell, to characterise the underlying drug release kinetics and diffusion characteristics of the formulations (Sharma et al., 2025a). The statistical significance of the various models discerned for both the formulations was calculated employing the standard values of R& F ratio (Dash et al., 2010).

2.11.5. Ex vivo permeation and retention studies

All animal studies were conducted after ethics approval: PU/45/99/CPCSEA/IAEC/2021/570. Excised Wistar rat abdominal skin was mounted on Franz cells (effective area 3.15 cm^2) with PBS: ethanol 80:20 v/v at 32 ± 0.5 °C (100 rpm) as receptor; LCZ-UDEs gel and MKT-LF cream (0.5g) were applied to the donor, and 1 mL receptor samples were collected over 24 h with immediate medium replacement, then quantified by validated HPLC method (n = 3). After 6 h, the skin was rinsed, minced, extracted in methanol (5 mL, 24 h at 32 ± 1 °C), filtered (0.22 μm), and analyzed by HPLC at 296 nm to determine drug retention. The extraction protocol was adopted from previously validated dermatokinetic methods reported for lipophilic drugs in rat skin (Makwana et al., 2025; Thakur et al., 2020).

2.11.6. Skin permeation imaging studies

Skin permeation was visualized using coumarin-6-loaded UDEs gel (0.15 μmol/mL dye substituting LCZ) prepared by the standard protocol. Coumarin-6, a lipophilic fluorescent probe with physicochemical properties similar to LCZ, was incorporated as a surrogate marker to enable visualization of vesicle penetration without affecting ethosomal characteristics. Dye-gel and free coumarin-6 solution were applied to 2 cm^2 shaved dorsal rat skin for 6 h, after which excised skin was PBS-rinsed, mounted, and imaged by confocal microscopy (Nikon Eclipse Ti, Nikon Instruments Inc., Melville, USA) atexcitation wavelength of 488 nm to assess intradermal fluorescence depth and distribution (Liu et al., 2025).

2.11.7. Dermatokinetic modelling

Dermatokinetics were evaluated *ex vivo* using Wistar rat skin mounted on a Franz diffusion cell, with 0.5 g formulation applied to the donor and PBS: ethanol (80:20 v/v) at 32 ± 0.5 °C as receptor under continuous stirring; at 0–12 h, skin was washed, heat-treated (60–80 °C, 3–6 s) to separate epidermis/dermis, minced, extracted in methanol (12 h), filtered (0.22 μm), and LCZ quantified by HPLC at 296 nm (n = 3 per time). Sampling intervals (0.5–12 h) were selected to adequately represent both absorption and elimination phases, allowing valid estimation of dermatokinetic parameters. Drug concentration-time profile in each layer were fitted to a one-compartment model to estimate K_p (dermal permeation constant), C_{max} (maximum skin concentration), K_e (skin elimination constant), T_{max} (time to Cmax), and $AUC_{0\text{-}12h}$ using PK Solver and spreadsheet analysis for parameter computation (Alshetaili et al., 2025).

2.12. In vitro anti-fungal studies

Clinical *Trichophyton rubrum* (NCPF 0263) was obtained from Culture collections, UK Health Security agency and was maintained on SDA with chloramphenicol at 28 ± 2 °C; 7–10-day conidia were collected in saline with 0.05% Tween 80, filtered, and standardized to 1–5 × 10^4 colony forming units (CFU)/mL as per CLSI guidance. Standardization employed hemocytometry and spectrophotometric calibration to ensure reproducible inocula for susceptibility testing. Antifungal activity of LCZ-UDEs, LCZ solution, and MKT-LF cream against *T. rubrum* followed CLSI M38-A2 in RPMI-1640/MOPS (pH 7.0), using two-fold dilutions from 2.0 to 0.00012 μg/mL in 96-well plates with 1–5 × 10^4 CFU/mL inocula and appropriate growth/sterility controls. Plates were incubated for 7 days at 28 ± 2 °C; OD600 quantified growth, and MIC was defined as the lowest concentration with visible inhibition versus the control in triplicate runs (Ghannoum et al., 2006; Santos and Hamdan, 2005). From MIC and higher concentration wells without visible growth, 20–50 μL aliquots were plated on drug-containing SDA, incubated 5–7 days at 28–30 °C, and examined for colonies. MFC was the lowest concentration, yielding 0 CFU, with MFC/MIC ≤ 4 indicating fungicidal and >4 fungistatic effects, tested in triplicate for reproducibility (Espinel-Ingroff et al., 2002; Mukherjee et al., 2003).

Dynamic killing was profiled at 0.5×, 1×, 2×, and 4× MIC (0.000125–0.001 μg/mL LCZ equivalents) for LCZ-UDEs, LCZ solution, and MKT-LF cream against ~1 × 10^6 CFU/mL *T. rubrum* in SDB. Cultures agitated at 28–30 °C were sampled at 0–24 h, serially diluted, plated on SDA, incubated for 5 days at 30 °C, and $\log_{10}$ CFU/mL enumerated (n =

6; triplicate assays) and the results were expressed as percent supression of growth at each time point to classify fungistatic versus fungicidal trajectories (Mukherjee et al., 2003; Yang et al., 2018).

2.13. Haemolysis assay

Haemolytic potential was assessed on sheep blood agar using wells loaded with Triton X-100 (positive control), LCZ-UDEs gel, MKT-LF cream, and water (solvent control), followed by incubation at 37 °C for 24 h and measurement of haemolysis zones (Sæbø et al., 2023).

2.14. Cell culture-based in vitro evaluation

HaCaT keratinocytes (NCCS, Pune) were grown in KGM with 10 % FBS, penicillin (100 U/mL), and streptomycin (100 µg/mL) at 37 °C, 5 % CO_2; at ~70 % confluence, cells were trypsinized and seeded for assays (96-well; 1×10^4 cells/well). MTT assessed cytotoxicity of LCZ solution, blank UDEs, and LCZ-UDEs: cells (5×10^3/well) were attached for 48 h, treated with 50 µg/mL for 48 h, incubated with MTT (0.5 mg/mL, 3 h), formazan solubilized in DMSO, and absorbance read at 570 nm to calculate viability versus untreated controls (triplicates) (Cataldi et al., 2022). Coumarin-6-labeled UDEs (equivalent to 50 µg/mL dye) were applied to HaCaT monolayers (12-well; 1×10^5 cells/cm^2) for 3 h at 37 °C, washed thrice with PBS, and visualized by fluorescence microscopy (GFP filter) to assess internalization qualitatively (Thiramanas et al., 2024). Phase-contrast microscopy was used to evaluate morphology after 48 h of exposure to LCZ solution, blank UDEs, or LCZ-UDEs (50 µg/mL), with PBS washes before and after treatment, comparing cell shape, attachment, and integrity to those of untreated controls (Sharma et al., 2021).

2.15. Skin irritation and safety evaluation

Female BALB/c mice were randomized into control, LCZ-UDEs gel, and MKT–LF cream groups; 0.5 g of each test was applied daily to a shaved 2 cm^2 dorsal area for 7 days. Erythema was scored daily using a 0–4 scale, where 0 = no erythema, 1 = slight (light pink), 2 = moderate (dark pink), 3 = moderate to severe (light red), and 4 = severe (dark red) as per Draize's skin irritation scoring method. At study completion, mice were euthanized, dorsal skin was fixed in 10 % buffered formalin, H&E-stained, and examined histologically for irritation or inflammation to compare dermal safety between LCZ-UDEs gel and the marketed cream (Sharma et al., 2025b).

2.16. Statistical analysis

Data are presented as mean ± standard deviation (SD). Group comparisons were analyzed by one-way ANOVA followed by Tukey's post hoc test, with $p < 0.05$ considered statistically significant. Statistical analyses were performed using GraphPad Prism (version 13.1), while Microsoft Excel 2013 was used for supplementary calculations.

3. Results and discussion

3.1. QbD-based development and optimization of LCZ-UDEs

Fig. S2 illustrates an Ishikawa fish-bone diagram showing the possible factors that could influence the quality attributes of the LCZ-UDEs formulation. Following identification of the key factors, an FMEA study was performed, as shown in Table S2, where five variables were assigned as high risk, each with RPN values of ≥ 800, *viz.,* phospholipid concentration (i.e., 900), ethanol concentration (i.e., 900), edge activator concentration (i.e., 900), type of phospholipid (i.e., 810), and type of edge activator (i.e., 810). These factors showed strong associations with vesicle size and PDE. The type of surfactant was identified as having a medium risk (RPN 448), while factors such as stirring speed (i.e., 80), stirring time (i.e., 48), and stirrer type (i.e., 18) were deemed to have low risk, with low RPN scores due to their minimal influence. These findings construed the selection of seven medium and high-risk factors for subsequent Taguchi screening and optimization.

3.2. Identification of critical variables through factor screening in LCZ-UDEs

To identify the most influential formulation and process variables impacting the CQAs of LCZ-UDEs, a Taguchi array-based factor screening study was conducted. The evaluation focused on vesicle size and PDE as the primary CQAs, as represented in Table S4. The standardized effects are visualized through Half-Normal plots and statistically ranked using Pareto charts (Fig. S3). For vesicle size, as shown in Fig. S3a, the Half-Normal plot demonstrated that ethanol concentration (Factor D) exhibited the most pronounced standardized effect, followed by PG concentration (B) and lipid concentration (A). The Pareto chart corroborated these findings, showing that Factor D exceeded even the Bonferroni-corrected t-value threshold, suggesting a statistically significant impact ($p < 0.01$). PG and lipid concentration, though, were found to lie below the Bonferroni limit, but remained above the standard t-value cutoff, indicating their practical significance in modulating vesicle size ($p < 0.01$). Regarding PDE, as depicted in Fig. S3b, the Half-Normal plot indicated that the lipid type (Factor F) was the most influential parameter, followed closely by PG concentration (B). The Pareto analysis reaffirmed these results, with both factors surpassing the Bonferroni limit, thus confirming their critical roles. Ethanol concentration and the type of edge activator, although statistically less dominant, showed a notable influence, suggesting that their cumulative contribution cannot be ignored. From the analysis above, three key MAs, namely the concentration of PL90G (lipid), the concentration of Span® 20, and ethanol content, were consistently identified as the most impactful variables influencing both the CQAs. These were, therefore, selected as the CMAs for subsequent optimization studies. Other factors, such as surfactant type and stirring speed, which demonstrated minimal effects below the statistical significance threshold, were maintained at predetermined levels during the optimization process (Waghule et al., 2021).

3.3. Design-driven systematic optimization of LCZ-UDEs

Based on the preceding risk assessment and factor-screening analyses, a Box-Behnken design (BBD) was employed to conduct a systematic optimization of the formulation. A total of 15 formulations of LCZ-UDEs were prepared according to the design and optimized for vesicle size (nm), % drug release, and PDE. Within the QbD framework, the formulation data were analyzed by fitting the response variables to a second-order quadratic polynomial model. The statistical significance of the quadratic model was determined to be extremely high ($p < 0.0001$).

Table 1
Values of CQAs of LCZ-UDEs formulations prepared as per Box-Behnken design.

Runs	PDE (%)	Vesicle size (nm)	Drug release (%)
1	90.4	221	58.67
2	81.34	230	51.45
3	69.45	410	47.58
4	72.87	350	48.96
5	41.45	470	16.36
6	93.56	196	61.67
7	39.56	421	17.86
8	42.71	402	19.53
9	88.19	180	60.57
10	85.09	398	57.67
11	64.94	367	43.37
12	91.23	210	64.71
13	79.34	245	52.34
14	89.54	327	58.46
15	84.34	356	55.68

Table 1 provides a comprehensive overview of the different parameters of all the prepared formulations of LCZ-UDEs, without any replication.

The quadratic polynomial equations (Eq. (2)) generated for the studied response variables, together with the ANOVA-produced statistical parameters, are detailed in Table S5.

$$Y = \beta_0 + \beta_1 X_1 + \beta_2 X_2 + \beta_3 X_3 + \beta_{12} X_1 X_2 + \beta_{13} X_1 X_3 + \beta_{23} X_2 X_3 + \beta_{11} X_1^2 + \beta_{22} X_2^2 + \beta_{33} X^2 \quad (2)$$

The statistical analysis yielded ten coefficients (β_0 to β_{33}), encompassing the intercept term (β_0), and different linear, quadratic, and interaction terms. The construction of response surface diagrams helped map the responses over the experimental space, making it easier to understand the effects of variables and their interactions.

The models exhibited a remarkable fit to the response variables, with adjusted R-squared values ranging from 0.9863 to 0.9893, and predicted R-squared values closely ranging from 0.9888 ($p < 0.0001$) to 0.9951 ($p < 0.0001$ each). The close agreement between the adjusted r and predicted r values with the actual model indicates a strong fit to the data. The models were determined to have negligible "lack of fit" values, which further corroborate the validity of the hypothesized model.

3.4. Optimization via response surface methodology (RSM)

RSM was applied as a statistical and mathematical tool to evaluate the influence of selected CMAs on the quality characteristics of the LCZ-UDEs formulation. In the present investigation, RSM was employed to investigate how the concentrations of phospholipid (PL 90G), Span® 20, and ethanol (in ethanol: PG mixture) affect key CQAs, such as vesicle size, PDE, and in vitro drug release (%). Initially, the perturbation plots were generated to assess the individual effect of each formulation component on the CQAs, while keeping other variables constant. Subsequently, 2D contour plots and 3D surface plots were used to visualize the interactive and nonlinear effects of formulation variables across the design space, providing a more comprehensive understanding of variable interactions and aiding in the optimization of the LCZ-UDEs system.

(i) Perturbation plots analysis

The perturbation plots, as seen in Fig. S4, provided a clear visualization of the individual effects of the CMAs, *viz.,* PL 90G (represented by line A), Span® 20 (line B), and ethanol: PG (line C), on the key CQAs of the LCZ-UDEs formulation, *viz.,* PDE, vesicle size, and percent drug release.

For PDE (Fig. S4. II), the plot revealed that PL 90G had the most significant influence, as evidenced by the steep curvature of its line. The drug entrapment efficiency initially increased with the increasing concentration of PL 90G. Still, it declined beyond the optimal range, indicating the necessity of a balanced phospholipid level to achieve maximum drug entrapment. Span® 20 and ethanol: PG showed a moderate yet positive effect, contributing to improved bilayer stability and efficient drug encapsulation.

The perturbation plot of vesicle size (Fig. S4.I) showed a distinct U-shaped curve for all three variables, suggesting that the vesicle size was minimized at the intermediate concentrations of each component. PL 90G and ethanol: PG exerted comparable effects, with their central levels favoring the formation of smaller vesicles, likely due to an optimal balance between bilayer rigidity and fluidization. Span® 20, which is a non-ionic surfactant, exhibited a subtler effect, aligning with its known role as an edge activator that modulates membrane flexibility and vesicle morphology (Sarolia et al., 2023).

In the case of drug release (Fig. S4.III), PL 90G again exhibited a dominant and nonlinear influence. Higher concentrations of PL 90G led to reduced drug release, possibly due to increased membrane thickness and reduced permeability. In contrast, Span® 20 and ethanol: PG contributed positively but less intensively, plausibly enhancing membrane fluidity and facilitating drug diffusion.

(ii) Response surface and contour plots

1. Effect on vesicle size

The influence of CMAs on the vesicle size was investigated using both 3D response surface plots and corresponding 2D contour plots. As shown in Fig. 1a (A), the interaction between PL 90G and Span® 20 exhibits a nonlinear "U-shape" trend. Vesicle size initially decreases with increasing concentrations of both components, reaching a minimum at their intermediate levels. Beyond this optimal point, the vesicle size increases again, possibly due to an excess of Span® 20 disrupting the lipid bilayer or inducing vesicle coalescence. Fig. 1a (B) explores the interaction between PL 90G and ethanol: PG mixture, revealing a similar trend. Mid-level concentrations of both components result in the smallest vesicles, likely due to ethanol's ability to fluidize lipid membranes and reduce their rigidity. The observed deviation from the expected monotonic trend, where vesicle size initially decreases and then increases with higher PL 90G levels, can be explained by the interplay between lipid concentration and bilayer dynamics. At lower PL 90G levels, the enhanced lipid availability promotes compact bilayer formation and efficient vesicle nucleation, resulting in smaller vesicles. However, beyond the optimal range, excessive PL 90G increases bilayer thickness and dispersion viscosity, which favors vesicle coalescence and enlargement. This nonlinear (U-shaped) pattern thus reflects the transition from a fluidized to a rigid bilayer regime, consistent with earlier observations for phospholipid-rich nanosystems. However, excessive ethanol may lead to vesicle swelling or instability, resulting in increased particle size (Limongi et al., 2021). Fig. 1a (C) demonstrates the combined effect of ethanol: PG and Span® 20, further supporting the observation that vesicle size is minimized when both components are used at moderate levels. Therefore, the plots highlight the importance of achieving a synergistic balance among lipid, edge activator, and solvent concentrations to obtain stable, nanosized vesicles with optimal characteristics.

2. Effect on PDE

The effect of CMAs on the PDE was analyzed using 3D response surface and 2D contour plots, as presented in Fig. 1b. In Fig. 1b (A), the interaction between PL 90G and Span® 20 is delineated, showing that the PDE increases with increasing concentrations of Span® 20 up to a certain point, after which a decline is observed. This indicates an optimal level of edge activator, i.e., Span® 20, that enhances vesicle flexibility and bilayer packing, promoting higher drug entrapment. However, excessive Span® 20 may destabilize the vesicular membrane, resulting in reduced entrapment. Fig. 1b (B) demonstrates the combined effect of PL 90G and ethanol: PG ratio, where PDE is maximized at intermediate levels of both components. Higher concentrations of PL 90G improve vesicle integrity and bilayer formation, while optimal ethanol: PG levels facilitate the solubilization of lipophilic drugs and enhance bilayer fluidity. Beyond this optimal range, vesicle destabilization or drug leakage may occur (Abdulbaqi et al., 2016). In Fig. 1b (C), the interaction between ethanol: PG and Span® 20 highlights a broad plateau where high PDE is achieved when both components are present in moderate amounts. Ethanol increases membrane fluidity, while Span® 20 enhances membrane permeability, both of which contribute synergistically to improved drug loading. However, deviations toward very low or very high concentrations of either factor lead to a decline in PDE, likely due to disrupted vesicle structure or leakage. PDE followed an inverted U-shaped (bell-shaped) trend, where maximal entrapment was observed at intermediate concentrations of the formulation components. The plots suggest that maintaining a balanced formulation with moderate levels of phospholipid, edge activator, and ethanol is key to achieving maximum drug entrapment efficiency.

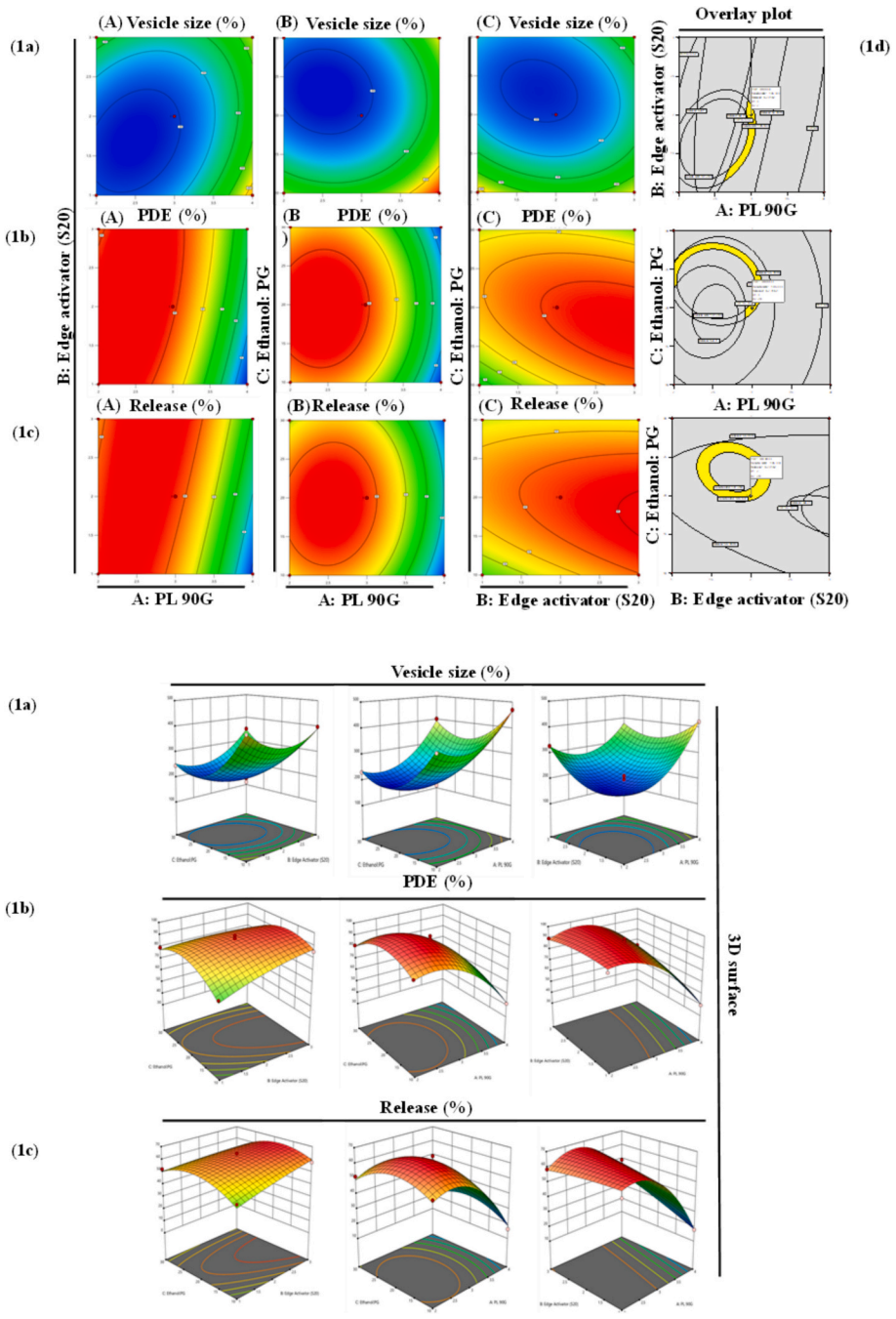

Fig. 1. 3D response surface and 2D contour plots display the effect of formulation variables, PL 90G, Span® 20, and ethanol: PG on CQAs: (a) vesicle size, (b) percent drug entrapment (PDE), and (c) percent drug release. Combinations assessed include: (A) Span® 20 vs. PL 90G, (B) ethanol: PG vs. PL 90G, and (C) ethanol: PG vs. Span® 20. (d) Overlay plots highlighting the optimal formulation zone within the defined design space, marked by the desirability flag.

3. Effect on percent drug release

The influence of formulation variables on the percentage of drug release (% release) from the LCZ-UDEs system was investigated using RSM, as depicted in the 3D surface and 2D contour plots (Fig. 1c). The key CMAs evaluated included the concentration of PL 90G, Span® 20 (edge activator), and the ethanol:PG ratio, selected based on prior screening studies. Fig. 1c (A) illustrates the interaction between PL 90G and Span® 20. A clear trend was observed: drug release increased with rising Span® 20 concentrations but decreased with increasing PL 90G. This could be attributed to the membrane-softening effect of Span® 20, which enhances bilayer flexibility and facilitates drug diffusion. Conversely, higher concentrations of PL 90G may result in a thicker and more rigid bilayer, restricting drug movement and reducing release efficiency (Khan et al., 2021).

In Fig. 1c (B), the interplay between PL 90G and ethanol: PG shows a similar pattern. Drug release peaked at intermediate levels of ethanol, likely due to ethanol's ability to fluidize lipid membranes and enhance drug solubilization and diffusion. However, at high PL 90G concentrations, the encapsulated drug may become more tightly retained within the lipid bilayer, leading to reduced release. Fig. 1c (C) highlights the combined effect of ethanol: PG and Span® 20. Increasing Span® 20 concentration resulted in significantly enhanced drug release, due to its role in disrupting the bilayer and promoting vesicle deformation. When ethanol was present at intermediate levels, it further enhanced bilayer fluidity and synergistically improved drug mobility. A plateau of high

release was observed at optimal concentrations of both Span® 20 and ethanol, reflecting their combined effect on maximizing release efficiency.

3.5. Search for an optimum formulation

Application of both graphical and numerical optimization approaches led to the identification of an optimal LCZ-UDEs formulation. The optimal region in the experimental design space was identified using overlay plotting, which further refined the constraints for the optimized formulation, as illustrated in Fig. 1d. Three distinct overlay diagrams were produced, each of which considered the conc. of PL 90G, Span® 20, and ethanol: PG. The details of the optimized formulation are depicted in the three overlay diagrams constructed between the concentrations. PL 90G, Span® 20, and ethanol: PG ($X_1 = 3$, $X_2 = 2$, and $X_3 = 20$).

In addition to the graphical method, the optimized formulation was further investigated using numerical optimization. The value of the desirability function, 'r' set to one, was applied to the constraints established for the desired target, and the entire experimental design was explored for compositions. Table S6 outlines the constraint set for numerical optimization, the excipients of various formulations, and the corresponding desirability values. The findings presented in Table S6 indicate that only one projected formulation satisfied the criteria. Consequently, the formulation linked to "Solution 5" was selected as the optimized formulation, achieving the highest possible magnitude of desirability function, i.e., 1.000. The selected formulation composition consisted of 3% PL 90G, 2% Span® 20, and 20% ethanol: PG. The selected formulation exhibited a combination of optimal values for all the studied variables, including a minimum vesicle size of 195.3 nm, a high EE of 91.0% and an optimum drug release of 62.3 %.

3.6. Measurement of particle size, polydispersity index (PDI), and zeta potential

The mean particle size of the final LCZ-UDEs formulation was recorded to be 197.0 ± 1.6 nm, thereby supporting its potential for enhanced transdermal delivery (Fig. 2A). Furthermore, the PDI of the formulation was recorded as 0.158 ± 0.03, indicating a narrow size distribution and high homogeneity within the vesicle population. This uniformity is desirable, as it contributes to formulation stability and consistent drug release behavior. The zeta potential of −20.5 ± 4.54 mV, as seen in Fig. 2B, indicates a moderately negative surface charge, which is sufficient to maintain colloidal stability by preventing vesicle aggregation. Similar zeta potential values have been reported for stable nanocarrier systems incorporating ethanol and surfactants, particularly in transdermal drug delivery formulations. These observations are in agreement with previously reported findings for ethanol-based deformable vesicles designed for topical application (Ansari et al., 2021).

3.7. Percent drug entrapment, drug payload, and vesicle quantification

The optimized LCZ-UDEs formulation demonstrated a high PDE of 91.0%, accompanied by a %DPL of 6.3%, both of which fall within the pharmaceutically acceptable limits. The substantial PDE can be attributed to the pronounced lipophilicity of LCZ, which favors its partitioning into the hydrophobic regions of the vesicular bilayer. Additionally, the elevated concentration of PL 90G contributes to the formation of a robust lipid matrix, facilitating efficient encapsulation of LCZ within the vesicular bilayer (Baghel et al., 2020). The vesicle count of unsonicated LCZ-UDEs was found to be 177,500 vesicles/mL, confirming a sufficient number of vesicles to enclose the drug molecule (Chouhan et al., 2021).

3.8. Evaluation of vesicle deformability

The deformability index (DI) of the optimized LCZ-UDEs formulation was found to be 0.85, confirming its high elastic nature. The vesicles were capable of traversing pores approximately twice as small as their mean size (197.0 nm), demonstrating sufficient flexibility to pass across the stratum corneum. This confirms the appropriate selection and concentration of Span® 20 and ethanol, which synergistically imparted membrane fluidity and deformability. Post-extrusion drug entrapment efficiency showed no significant reduction compared to the non-extruded formulation, indicating vesicle integrity was maintained during deformation. According to the literature, deformable vesicles in the range of 100–300 nm are considered ideal for effective skin penetration (Cevc and Vierl, 2010). The inclusion of Span® 20 effectively enhanced membrane flexibility, consistent with prior studies (Song et al., 2019). Additionally, the ethanol-induced bilayer fluidization further contributed to the deformability, allowing vesicles to squeeze through intercellular pathways without compromising their structure or drug payload.

3.9. Thermal and spectroscopic analysis

The thermograms of pure LCZ, individual excipients (PL 90G, ethanol, Span® 20, PG), and the final LCZ-UDEs formulation are illustrated in Fig. S5. A sharp endothermic peak at 151.98 °C, corresponding to the melting point of pure LCZ, was evident in the DSC thermogram, confirming its crystalline nature and purity. PL 90G, ethanol showed endothermic peaks at 230.6 °C and 82.77 °C, and Span® 20, PG showed peaks at 35.06 °C and 163.2 °C respectively, consistent with their expected thermal transitions, indicating their individual phase behavior.

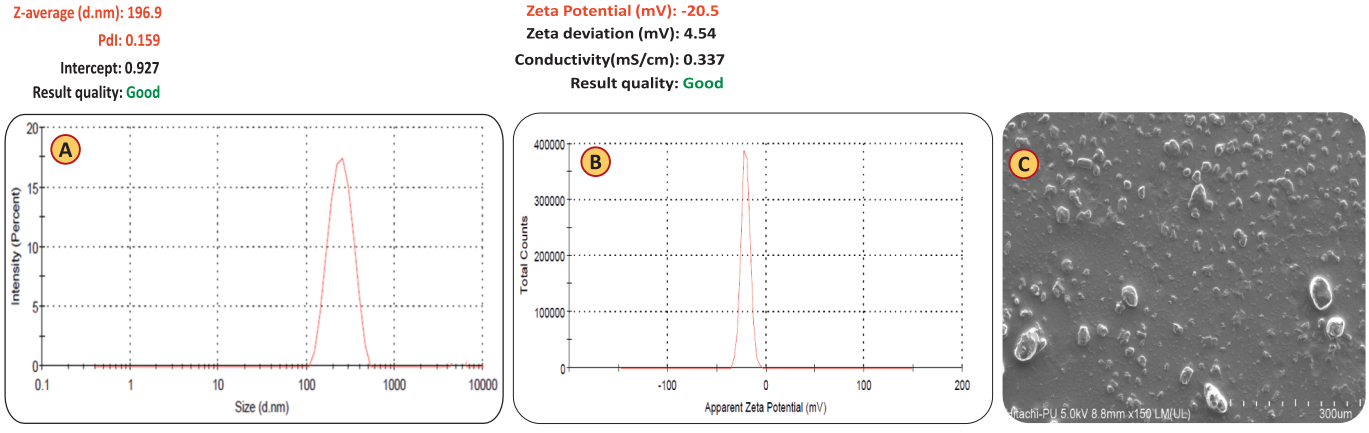

Fig. 2. (A) Vesicle size and PDI; (B) Zeta potential; (C) FESEM photomicrograph of LCZ-UDEs formulation at 150x.

In contrast, the LCZ-UDEs formulation exhibited a broad endothermic transition at 118.93 °C, distinctly different from that of the pure drug. This shift and broadening of peaks suggest a reduction in crystallinity and possible molecular dispersion of LCZ within the lipid bilayer. Absence of the characteristic LCZ melting peak in the LCZ-UDEs thermogram indicates potential drug-excipient interaction (s) and successful entrapment of LCZ within the vesicular system. These observations support the formation of a stable, homogeneous formulation with modified thermotropic properties resulting from the integration of all components (Shaikh et al., 2022).

The FTIR studies were employed to assess the potential interactions between LCZ and the excipients used during the formulation of LCZ-UDEs (Kumar et al., 2020). Fig. S6 presents the spectra of individual components and the optimized formulation: LCZ (A), PL90G (B), propylene glycol (C), Span® 20 (D), ethanol (E), and LCZ-UDEs formulation (F). The spectrum of LCZ (A) displayed characteristic absorption bands, including a broad aromatic C–H stretching vibration between 3050 cm^{-1} and 3000 cm^{-1}, aliphatic C–H stretching peaks between 2980 and 2850 cm^{-1}, a sharp C≡N (nitrile) between 2250 and 2180 cm^{-1} corresponding to the imidazole ring, aromatic C=C stretching at 1511 and 1424 cm^{-1}, and C–F/C–N stretching bands between 1215 and 1025 cm^{-1}, thus ratifying the structural integrity and purity of the drug. PL90G (B) exhibited a broad O–H stretching band around 3409 cm^{-1} and a strong ester carbonyl (C=O) peak near 1735 cm^{-1} and PO_2^- asymmetric stretching at 1238 cm^{-1}, consistent with its phospholipid nature. The spectrum of propylene glycol (C) showed O–H stretching at 3368 cm^{-1}, along with aliphatic C–H stretching between 2930 and 2850 cm^{-1} and C–O stretching in the region of 1150–1050 cm^{-1}. Span® 20 (D) demonstrated a broad O–H stretch around 3403 cm^{-1}, CH_2 stretching between 2920 and 2850 $cm^{-1}$and multiple C–O–C and ester-associated vibrations. Ethanol (E) showed O–H stretching at 3362 cm^{-1} and C–H bending vibrations around 1385–1052 cm^{-1}. In the spectrum of LCZ-UDEs formulation (F), the intensity of the nitrile peak (C≡N) was significantly diminished, the lipid ester C=O experienced a shift from 1735 to 1640 cm^{-1}, and the PO_2^-/C–O region (1240–1085 cm^{-1}) exhibited broadening. The extensive O–H band showed an increase as a result of PG and ethanol. The findings suggest that lulicoconazole is primarily encapsulated within the UDEs bilayer and engages in non-covalent interactions (such as hydrogen bonding or electrostatic interactions) with lipid head groups, all while maintaining its chemical integrity.

3.10. Microscopic characterization by FE-SEM

The morphological attributes of the LCZ-UDEs were observed using FESEM at 130 k × magnification, as shown in Fig. 2(C). The micrograph revealed intact, well-defined spherical vesicles with smooth surfaces. The structural integrity and smooth appearance of the vesicles reflected the role of phospholipids in forming a flexible and coherent bilayer that encapsulates the lipophilic core. The absence of surface cracks or deformation further supports the robustness of the vesicular membrane (Mehmood et al., 2024).

3.11. Evaluation of the LCZ-UDEs gel formulation

3.11.1. pH measurement and physical stability assessment

The magnitude of pH is a critical parameter for ensuring biocompatibility and non-irritant behaviour of a topical preparation. The pH of the optimized LCZ-UDEs gel, as observed in the current studies, was 6.0 ± 0.2, which falls within the normal range of human skin pH (4.5–6.4), validating its compatibility and suitability for dermal application. The formulation also exhibited excellent physical stability over a period of four weeks at room temperature, with absolutely no signs of discoloration, odour change, phase separation, or drug crystal formation. The gel maintained its consistency throughout the study, indicating excellent rheological stability of the gel formulation (Kuo et al., 2020).

3.11.2. Flow behavior analysis and texture profile

The explicit microrheological data obtained from the final formulation were evaluated employing a cone and plate viscometer and fitted to the Herschel-Bulkley model. The LCZ-UDEs gel demonstrated pseudoplastic (i.e., shear-thinning) behavior, as indicated by a flow behavior index (n) of 0.256 (Fig. 3A), and the MKT-LF cream exhibited a similar flow pattern with an "n" value of 0.262 (Fig. 3B), suggesting that both the formulations resist flow better at higher shear rates. The corresponding plots of shear stress and viscosity versus shear rate (Fig. 3C and D) further support this, showing a distinct decline in viscosity with increasing shear rate, an indication of good spreadability under mechanical stress.

The yield stress, representing the minimum stress required to initiate flow, was observed to be markedly (i.e., 2.9 times) higher in the LCZ-UDEs gel (i.e., 232.6 Pa) than that of the MKT-LF cream (i.e., 78.6 Pa), suggesting the involvement of a more structured gel matrix in the developed formulation. Besides, the consistency index (K) was also 2.3 times higher for the LCZ-UDEs gel (i.e., 233.95 $Pa{\cdot}s^n$) vis-a-vis the MKT-LF cream (i.e., 99.48 $Pa{\cdot}s^n$), implying greater internal resistance to flow. The increased viscosity of the LCZ-UDEs gel is expected to contribute positively to its prolonged skin retention, enhanced application comfort, and potential stability during storage. The findings indicate that the LCZ-UDEs gel exhibits superior rheological properties, which are considered quite favorable for topical administration (Garg et al., 2017).

Fig. 3 E and F depict the texture profile of the final LCZ-UDEs gel and MKT-LF cream, including firmness, consistency, cohesiveness, and index of viscosity. The LCZ-UDEs gel formulation exhibited distinctly superior gel strength (i.e., 2296.27 g), convenient spreading (i.e., 3053.26 g.sec), and extrusion from tubes (i.e., −1099.18 g), compared to MKT-LF cream, which showed gel strength (i.e., 5821.86 g), ease of spreading (i.e., 4267.08 g.sec), and extrusion from tubes (i.e., −4123.82 g). The formulation also demonstrated adequate cohesiveness, a crucial characteristic for maintaining the formulation at the intended application site. Furthermore, the curve uniformity also confirmed the even texture of the gel, affirming the absence of grittiness or clumps within the formulation. Thus, overall, the developed LCZ-UDEs gel formulation met all requisite textural criteria for any topical formulation (Sharma et al., 2018).

3.11.3. Evaluation of formulation stability

During the six months of stability evaluation at 5 ± 3°C (refrigerated) and at 40 ± 2°C/75 % ± 5 % RH (accelerated), the LCZ-UDEs gel formulation preserved its physical properties; no changes in colour, odour, grittiness, phase separation, or consistency were observed under either condition (Table S7). The pH values remained within a dermally acceptable range (i.e., 4.5–6.4), further indicating formulation compatibility for topical application. Correspondingly, the drug content data presented in Table S7 confirmed that the LCZ-UDEs gel remained chemically stable in each of the tested conditions. However, a slight reduction in the drug assay was recorded as the study progressed at elevated temperatures. After six months, the drug loss reached 2.46% at 40 ± 2°C/75 % ± 5 % RH, compared to a negligible loss of 1.52 % under refrigerated storage. This decline at higher temperatures is rationally attributed to the thermally induced destabilization of the vesicular system, leading to minor structural alterations in the lipid bilayers and, consequently, affecting drug retention. Although elevated temperatures may accelerate vesicle fusion and ethanol loss, the LCZ-UDEs gel exhibited only minimal changes under accelerated conditions, indicating satisfactory thermostability conferred by the combined stabilizing effects of ethanol, PG, and the Carbopol matrix. These results suggest that the LCZ-UDEs gel formulation demonstrates promising physical and chemical stability, with better retention of drug content at lower temperatures (Sharma et al., 2023). Accordingly, to ensure optimal shelf life and formulation performance, storage under refrigerated conditions is recommended, although room temperature conditions are still considered acceptable within the pharmacopeial limits. Although elevated

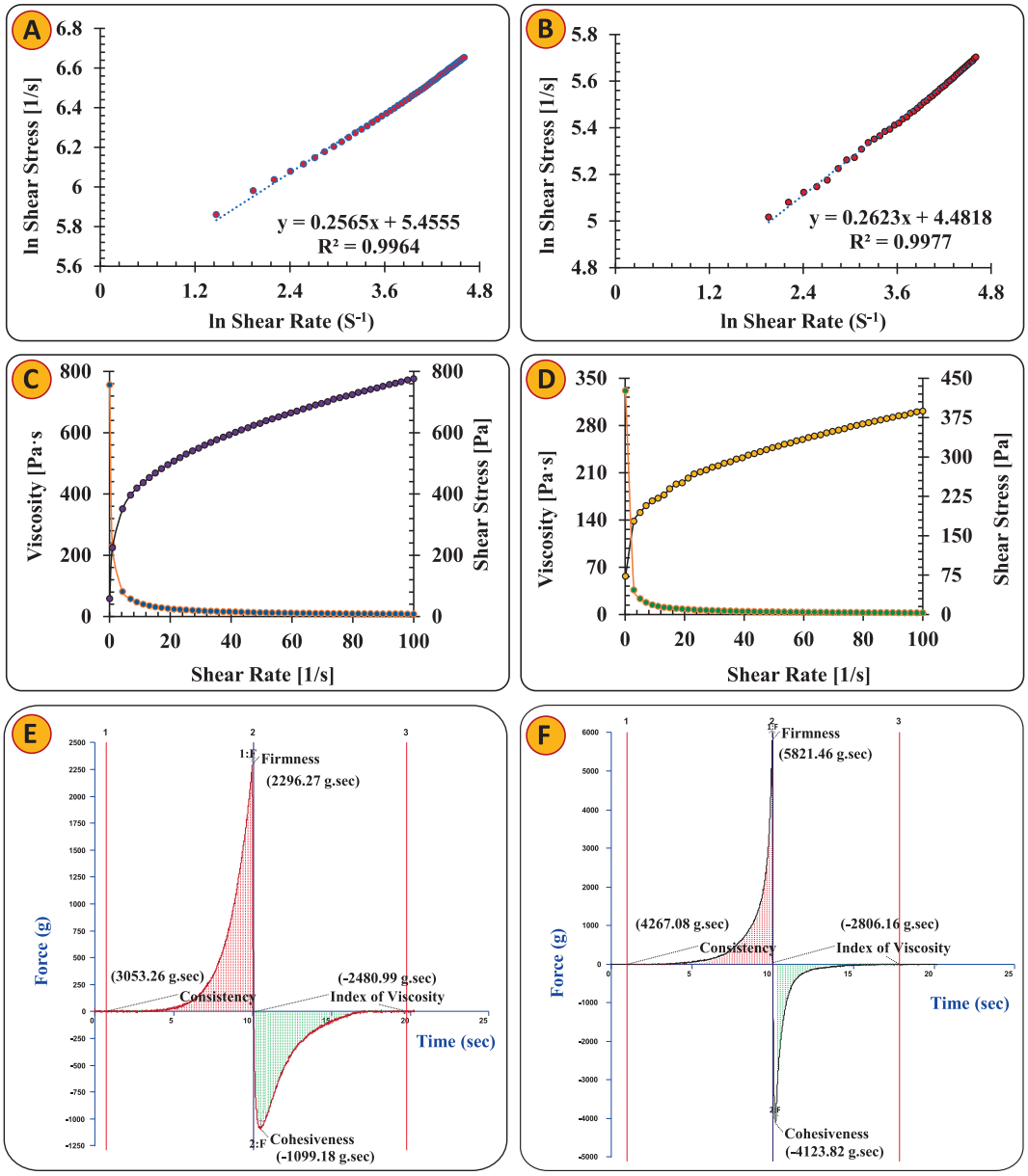

Fig. 3. Herschel-Bulkley plots present the relation between ln (shear stress) and shear rate for the LCZ-UDEs gel (A) and MKT-LF cream (B). The graphs illustrate the relationship between shear rate, viscosity, and shear stress for LCZ-UDEs gel (C) and MKT-LF cream (D). The texture profiles show the firmness, consistency, cohesiveness, and viscosity index for LCZ-UDEs gel (E) and MKT-LF cream (F).

temperatures may accelerate vesicle fusion and ethanol loss, the LCZ-UDEs gel exhibited minimal change under accelerated conditions, indicating satisfactory thermostability conferred by ethanol-PG-Carbopol interactions.

3.11.4. In vitro release and kinetic modelling

The in vitro drug release profiles of LCZ-UDEs and LCZ-UDEs gel demonstrated a distinct biphasic pattern, comprising an early burst release phase followed by a sustained release phase (Fig. 4). During the initial 10 h, LCZ-UDEs exhibited a significantly higher burst release (52.57% ± 6.54), compared to the LCZ-UDEs gel (42.01% ± 4.67). This rapid initial release may be attributed to loosely bound LCZ associated with or adsorbed near the vesicle surface and the enhanced diffusion of drug through the highly deformable phospholipid bilayers (El Maghraby et al., 2008). Conversely, the reduced burst effect in the gel formulation is likely a consequence of the increased diffusional resistance and steric hindrance imparted by the Carbopol gel matrix, which restricts vesicle mobility and retards drug diffusion during the early phase of release (Thakur et al., 2018). Following the burst phase, both formulations displayed gradual and sustained LCZ release over 48 h. The cumulative release from LCZ-UDEs reached 99.35%, whereas LCZ-UDEs gel released 72.76% which is significantly higher than that of UDEs gel ($p < 0.01$), confirming the role of the gel base as a secondary rate-modifying barrier. The slower release from the gel matrix supports prolonged drug residence and local retention, an attribute highly desirable for topical antifungal therapy, where sustained exposure at the infection site is required to inhibit fungal proliferation and reduce dosing frequency (Dave et al., 2020; Kaur et al., 2020; Shah et al., 2023).

To elucidate the underlying release mechanism, the release data were fitted into popular kinetic models, as presented in Table 2. The Korsmeyer-Peppas model demonstrated the highest correlation for both the formulations ($R = 0.9958$ for LCZ-UDEs; $R = 0.9868$ for LCZ-UDEs gel $p < 0.00001$ each), indicating that this model best explains the drug release behaviour. Additionally, the Korsmeyer-Peppas model was

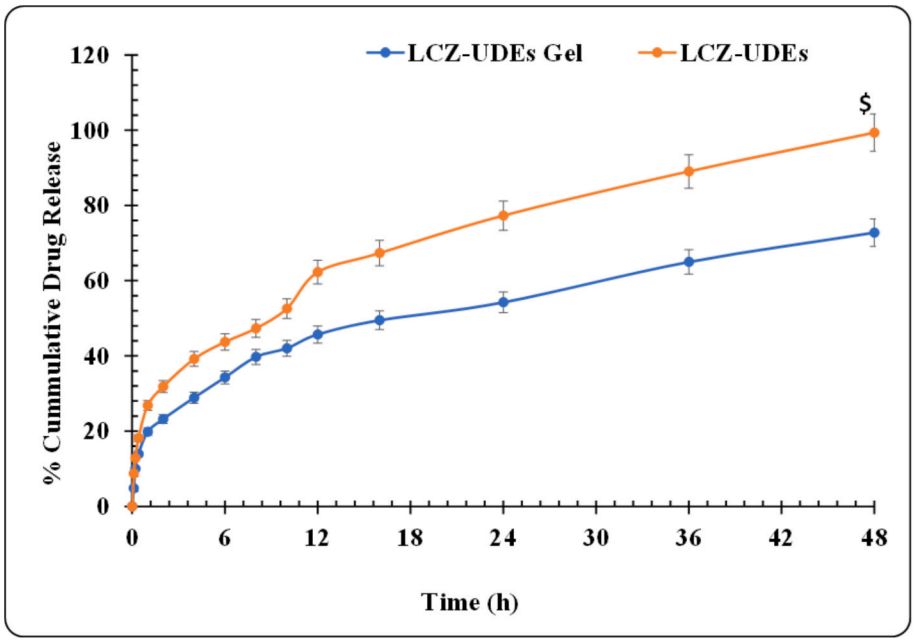

Fig. 4. In vitro release profile of LCZ from LCZ-UDEs-gel and LCZ-UDEs. Each bar indicates ± SD (n = 3); $ signifies $p < 0.01$ (UDEs vs. UDEs gel).

Table 2
The values of the correlation coefficient and the statistical significance thereof from various drug release kinetics models.

Release Kinetic Model	LCZ-UDEs			LCZ-UDEs Gel		
	(R)	F-Ratio	P<	(R)	F-Ratio	P<
Korsmeyer-Peppas	0.9958	118.30	0.00001	0.9868	37.13	0.001
Higuchi	0.9912	56.07	0.00001	0.9863	35.75	0.001
Hixson-Crowell	0.9928	68.70	0.00001	0.9774	21.38	0.001
First-order	0.9028	4.41	ns	0.8927	3.92	Ns
Zero-order	0.9634	12.92	0.01	0.9496	9.18	0.01

*ns: not significant.

applied to determine the drug release mechanism from the matrix system. In this model, an n value less than 0.45 indicates Fickian diffusion, while values between 0.45 and 0.89 suggest that the drug release follows an anomalous transport mechanism involving both diffusion and polymer swelling (Ahuja et al., 2007). The strong fit of the release profiles to the Korsmeyer-Peppas mode yielding "n" values of 0.7884 and 0.7484 for LCZ-UDEs gel and LCZ-UDEs, respectively, imply anomalous (i.e, non-Fickian) transport, a combination of diffusion and swelling/erosion mechanisms of drug release. The Higuchi model also yielded excellent linear correlation values (for UDEs, $R = 0.9912$; $p < 0.00001$ and for LCZ-UDEs gel, $R = 0.9863$; $p < 0.001$), substantiating that the drug release is predominantly governed by Fickian diffusion through a matrix-type system (Pople and Singh, 2011).

Also, statistically significant values of the correlation coefficient obtained for the Hixson-Crowell and zero-order models, $p < 0.01$–0.00001, suggest that LCZ release is neither constant over time nor governed primarily by vesicle erosion or dimensional changes. Collectively, both the correlation analysis and statistical evaluation strongly support that the Korsmeyer-Peppas model provides the most accurate and mechanistically relevant description of LCZ release from both UDEs and UDEs gel. Similarity between the correlation coefficients obtained with LCZ-UDEs and LCZ-UDEs gel reflects the uniformity and structural consistency of the formulations, suggesting minimal interference from swelling, erosion, or polymer relaxation phenomena after incorporation into the gel matrix (Dash et al., 2010; Higuchi, 1963).

3.11.5. *Ex vivo permeation and retention studies*

Fig. 5 A shows the percent drug permeated versus time for LCZ-UDEs gel formulation *vis-à-vis* MKT-LF cream. It is evident from the observed findings that the transportation of the drug in LCZ-UDEs gel (29.8 % ± 4.8) was 2.4-fold higher than that of MKT-LF cream (12.4 % ± 3.8), confirming the superiority of new lipid-based formulations. The LCZ-UDEs gel formulation exhibited a notably higher level of permeation ($p < 0.0001$) than that observed with the MKT-LF cream. The advanced drug transport characteristics are attributed to the interface between bio-compatible components (PLs) with the skin, leading to improved penetration. The findings suggest that PLs exhibit a distinct ability to enhance tissue hydration due to their unique property of forming lamellar structures, leading to an augmentation in drug permeation (Hassan et al., 2023; Mahmood et al., 2022).

Fig. 5B illustrates the quantity of drug retained within the skin layers, and suggests markedly superior drug retention by LCZ-UDEs gel (i.e., 436.4 g/cm^2 ± 11.8) as compared to MKT-LF cream (i.e., 38.4 g/cm^2 ± 9.6), which may be ascribed only to formulation-mediated characteristics of the former. In a nutshell, improved drug deposition results from increased permeability. Consequently, the LCZ-UDEs gel achieved an 11.3-fold higher level of drug deposition compared to the MKT-LF cream. The research strongly demonstrated that UDEs not only enhanced the permeability of the drug molecule but also played a stellar role in enhancing its retention within the skin, in agreement with earlier studies (Sharma et al., 2024). The prolonged presence of the drug indicated that the LCZ-UDEs gel formulation served as an effective drug reservoir, while retaining the drug formulation within its gaps to enable extended drug release (Niu et al., 2022).

3.11.6. *Skin permeation imaging studies*

As shown in Fig. 5, the CLSM images clearly demonstrate the successful permeation of the fluorescently labelled vesicles of the UDEs gel into the tough skin layers. The fluorescent image (Fig. 5D) reveals discrete circular green fluorescent spots, indicating the presence of coumarin-6-loaded ethosomes distributed throughout the skin matrix. These spots represent intact vesicles that were able to pass through the stratum corneum and localize within the basal regions of the epidermis. The overlay image (Fig. 5C), which combines fluorescent and differential interference contrast (DIC) imaging, highlights the co-localisation of the vesicles within the skin architecture, thus construing their structural

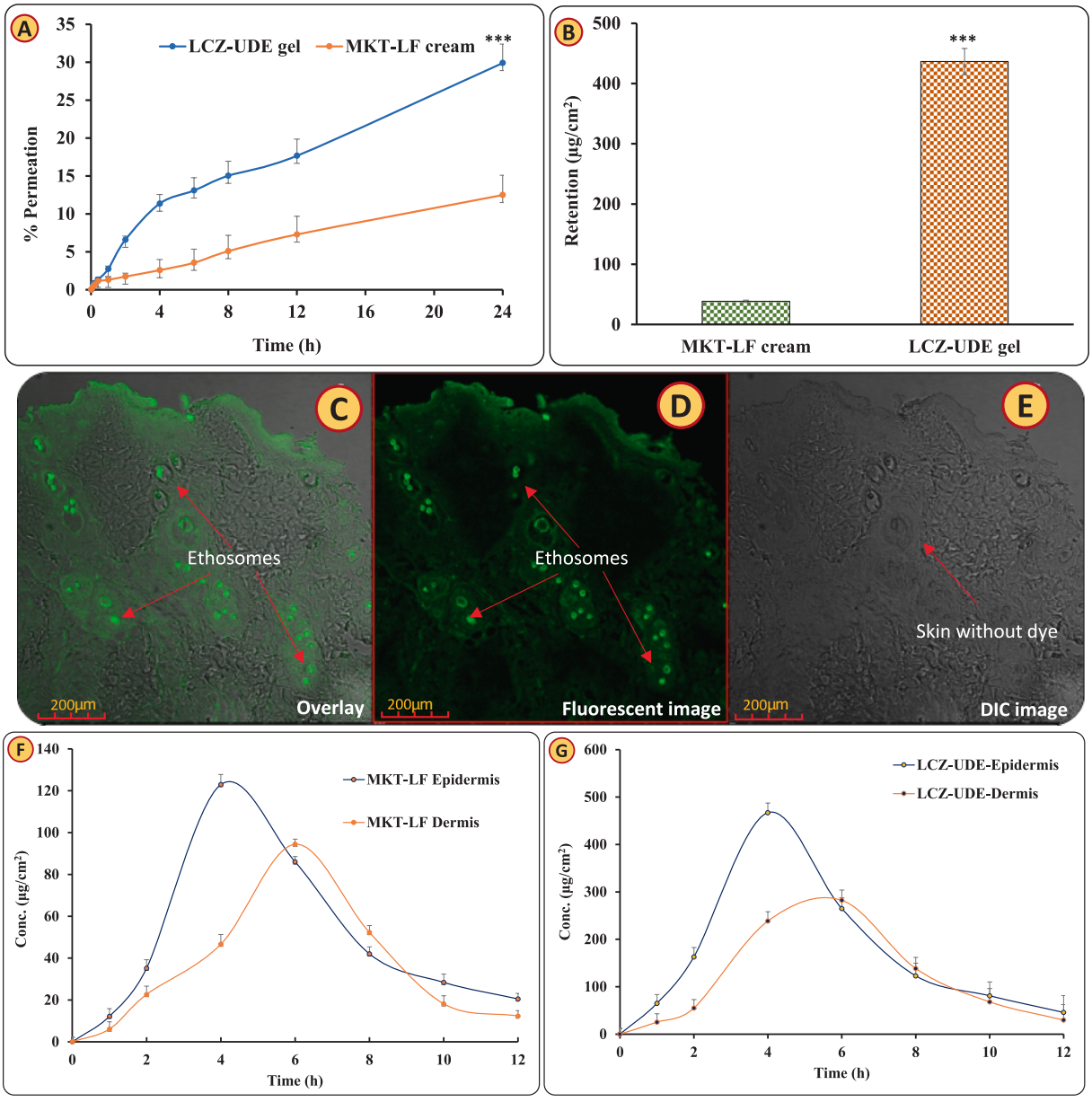

Fig. 5. (A) *Ex vivo* permeation profile of LCZ-UDEs gel formulation andMKT-LF cream formulation (B) Bar diagram for the amount of LCZ deposited in the skin for LCZ-UDEs gel formulation and MKT-LF cream formulation. Each bar indicates mean ± SD (n = 3). The denotion *** indicates a highly significant difference ($p < 0.0001$) in the permeation and retention studies between the LCZ-UDEs gel formulation and MKT-LF cream. (C) Combined overlay of fluorescent intensity with the differential interference contrast (DIC) confocal image of the skin treated with coumarin-6 loaded UDE gel (D) Fluorescent intensity of the skin treated with the coumarin-6 loaded UDEs gel; (E) DIC image of skin without dye after a 6-h application of the coumarin-6-loaded UDEs gel. *Ex vivo* dermatokinetic profiles illustrating drug concentrations in (F) the epidermis and dermis after application of the LCZ-UDEs gel and (G) the epidermis and dermis after application of the MKT-LF cream. Each crossbar represents the mean ± SD (n = 3).

integrity and enhanced permeation potential. In contrast, the DIC image (Fig. 5E), taken from a control sample without dye, shows no fluorescent signal, thereby validating the specificity and effectiveness of vesicle-mediated delivery. The results strongly substantiate the role of UDEs vesicles in facilitating enhanced transdermal delivery by improving penetration depth and uniform distribution across the skin layers.

3.11.7. Dermatokinetic modelling

Dermatokinetic profiles of LCZ-UDEs gel within the epidermal and dermal layers of Wistar rats were determined using a one-compartment open model, which monitored drug distribution within the skin layers at short time intervals following a single topical *ex vivo* application, as shown in Fig. 5F and 5G. The LCZ-UDEs gel formulation displayed a notably increased level of significance relative to the MKT-LF cream. Various important dermatokinetic parameters, like $AUC_{0\text{-}12h}$, C_{max}^{skin}, T_{max}^{skin}, K_e (skin elimination rate constant), and K_p (skin permeation rate constant), were assessed (Nirbhavane et al., 2018) as seen in (Table S8). The findings made it quite evident that the LCZ-UDEs gel formulation in the SC elevated the half-life of the LCZ. A significant reduction was observed in the values of T_{max}, whereas C_{max} in the dermis and epidermis, as well as AUC in the dermal layer, exhibited intense magnification. Consequently, the data revealed a higher capacity of the LCZ-UDEs gel formulation for augmenting LCZ transport through the layers of skin compared to the MKT-LF cream (Bhargav et al., 2021).

3.12. In vitro anti-fungal studies

The MIC of the LCZ-UDEs formulation was recorded at 0.00025 μg/mL, while the LCZ-SUS and MKT-LF cream exhibited MIC values of 0.0005 μg/mL and 0.001 μg/mL, respectively. These results indicate that the LCZ-UDEs exhibit enhanced antifungal efficacy as compared to both the LCZ-SUS and the MKT-LF cream formulation. The MIC value of 0.00025 μg/mL for LCZ-UDEs aligns well with previously reported MIC_{50} values for LCZ against *T. rubrum*, which typically range between 0.00012 and 0.0005 μg/mL, confirming the exceptional potency of LCZ and supporting the validity of the observed results (Wiederhold et al., 2014).

The MFC for LCZ-UDEs was observed at 0.0005 μg/mL, whereas free LCZ and MKT-LF cream required much higher concentrations of 0.001 μg/mL and 0.002 μg/mL, respectively, to achieve the fungicidal activity. The ratio of MFC/MIC for LCZ-UDEs was determined to be 2, which is consistent with fungicidal behavior, as ratio of ≤4 typically indicates fungicidal effect (Maeda et al., 2016). In contrast, higher MFC/MIC ratios for the marketed cream suggest a fungistatic effect rather than fungicidal nature at clinically relevant concentrations. These findings, thus, unequivocally ratify that the LCZ-UDEs formulation exhibits significantly enhanced antifungal action than either the free drug or the MKT cream, and thus would have superior efficacy in eradicating the infection. The enhanced antifungal potency of LCZ-UDEs can be attributed to their superior skin penetration, prolonged drug residence at the infection site and improved interaction with fungal cell membranes (Espinel-Ingroff et al., 2002). The UDEs vesicles, composed of PL 90G, ethanol, and Span® 20, possess high deformability and lipid compatibility, enabling efficient passage through stratum corneum lipid channels and enhanced localization of LCZ at infection sites. PL 90G, being structurally analogous to biological membrane lipids, promotes vesicle-membrane fusion and facilitates LCZ transfer into ergosterol-rich fungal membranes. Concurrently, ethanol and Span® 20 induce transient lipid fluidization in both vesicular and fungal membranes, increasing membrane permeability and accelerating LCZ partitioning into the fungal cell. As a result, LCZ reaches the intracellular target enzyme (lanosterol 14-α-demethylase) more effectively, intensifying ergosterol depletion and membrane destabilization. This mechanism aligns with previously reported findings, where ethosomal and other soft-vesicle carriers demonstrated enhanced cutaneous drug deposition and improved antifungal efficacy compared with conventional formulations due to their superior membrane interaction and penetration capabilities (Dave et al., 2020; Marto et al., 2016; Touitou and Natsheh, 2024).

Fungal viability was measured as $\log_{10}$ CFU/mL, and, for interpretation, these counts were compared with the untreated growth control. Fig. 6 shows that at 0.5 × MIC (0.000125 μg/mL) all treatments suppressed fungal proliferation relative to the control, with LCZ-UDEs producing the most rapid and pronounced early killing, limiting viable counts to < 40% of the control within 4 h. By 24 h, LCZ UDEs (76.2 ± 1.13% of control counts) continued to exhibit substantial suppression ($p < 0.001$), outperforming the MKT-LF cream (63.3 ± 1.10%, $*p < 0.01$) and the LCZ-SUS (52.03 ± 0.58%, $\#p < 0.05$). At 1 × MIC, LCZ UDEs again achieved superior early-phase killing, reducing viable counts to < 30 % of control by 4–8 h, and by 24 h remained at 56.2 ± 0.72% of control, indicating a sustained antifungal effect likely attributable to the slow release of drug from the ultra-deformable vesicles. In contrast, the MKT-LF cream and LCZ-SUS showed more rapid rebound growth, with

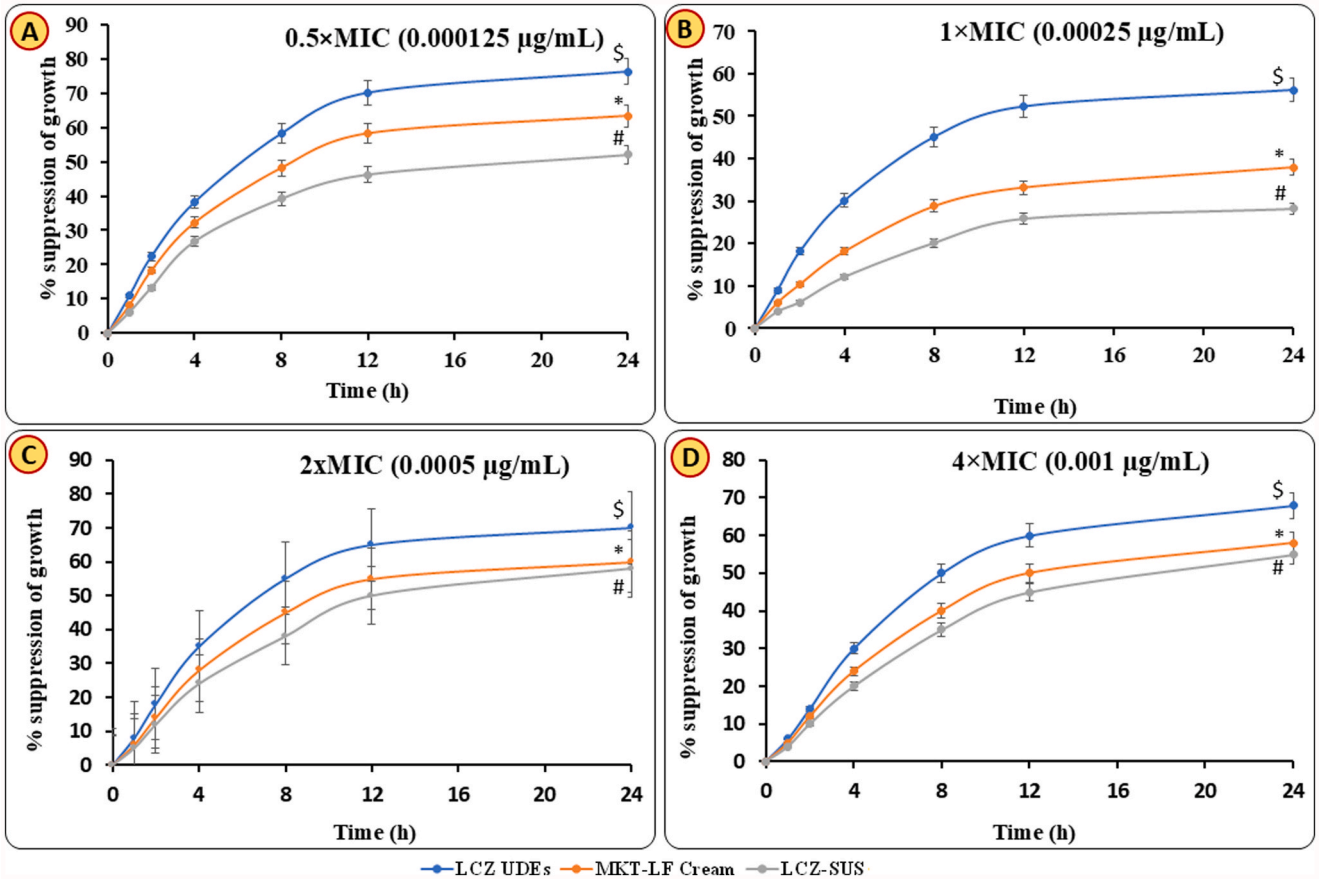

Fig. 6. Time-kill curves showing percent suppression of growth of *T. rubrum* over 24 h at (A) 0.5 × MIC, (B) 1 × MIC, (C) 2 × MIC, and (D) 4 × MIC of LCZ. Data are represented as mean ± SD (n = 3), $p < 0.001 indicates a highly significant difference between growth control and LCZ-UDEs formulation, *p < 0.01 represents a significant difference between growth control and MKT-LF cream, while #p < 0.05 represents no significant difference between growth control and LCZ-SUS.

lower residual inhibition between 8 and 24 h. At 2 × MIC and 4 × MIC, LCZ UDEs maintained strong early and mid-phase fungistatic effects, reducing viable counts to < 35% of control by 8 h and sustaining significant suppression through 24 h (70.1 ± 0.13% and 68.01 ± 1.12%, respectively; $p < 0.001$). These findings agree with previously reported time-dependent killing profiles of LCZ UDEs (Ashraf et al., 2018).

3.12.1. Haemolysis assay

As depicted in Fig. S7, Triton X-100 produced a distinct haemolysis zone of approximately 10–12 mm in diameter, confirming the assay's sensitivity. In contrast, the LCZ-UDEs formulation, MKT-LF cream, LCZ-SUS, and water showed no observable haemolysis zones, indicating the absence of red blood cell lysis. These results ratify that the LCZ-UDEs formulation is non-haemolytic and haemocompatible. These results suggest that the formulation components do not disrupt red blood cell membranes and are safe for dermal use. Overall, the non-haemolytic nature of LCZ-UDEs supports its biocompatibility and suitability for topical or transdermal application, consistent with earlier findings on ethanol-based vesicular systems (Saroj et al., 2024).

3.13. Cell culture-based in-vitro evaluation

Fig. 7a shows the outcome of the MTT-based cell viability test performed on HaCaT cells to assess the cytotoxic potential of the formulated LCZ-UDEs. The untreated HaCaT cells served as the control group, representing 100% viability. Following 48 h of treatment, the developed LCZ-UDEs formulation and the blank UDEs formulation (i.e., without drug) showed no notable cytotoxic effects at a level of 50 μg/mL, with cell viabilities of 91.4 ± 3.2% and 92.4 ± 3.8%, respectively. In contrast, the LCZ-SUS resulted in a marked reduction in cell viability, yielding only 35.4 ± 2.6% viability compared to the control. These results unambiguously revealed that the LCZ-UDEs formulation did not exert any harmful effect (s) on HaCaT cells. A marked statistical variation ($p < 0.001$) was observed when comparing the control group with the LCZ-SUS group. In contrast, no statistically notable change ($p > 0.05$) was observed when the control was compared with either the LCZ-UDEs or the blank formulation. The comparable viability profiles of blank UDEs and LCZ-UDEs can be attributed to the mild membrane-fluidizing effect of ethanol and Span® 20 within the vesicles, which may contribute to minimal baseline cytotoxicity while remaining within acceptable biocompatible limits (Bnyan et al., 2018). Under the short exposure period of the in vitro assay, LCZ is released gradually from the vesicles, resulting in no additional cytotoxic effect relative to blank UDEs (Nosratabadi et al., 2024). This observation is consistent with earlier reports highlighting the high biocompatibility of phospholipid-ethanol vesicular systems and indicates that the carrier does not potentiate drug-induced toxicity (Touitou et al., 2000). Together with the absence of dermal irritation observed in the in vivo study (Section 3.16), these findings confirm the safety and suitability of LCZ-UDEs for topical application.

Fig. 7b (A) represents cells treated with the free coumarin-6 dye alone, which exhibited weak and diffused fluorescence, indicating limited permeation and uptake by passive diffusion. In contrast, Fig. 7b (B) demonstrates a pronounced green fluorescence within the cytoplasm of HaCaT cells treated with coumarin-6-loaded LCZ-UDEs formulation, signifying efficient internalization and distribution of the vesicular system.

This disparity in uptake efficiency highlights the advantage of the LCZ-UDEs delivery system. The encapsulated dye enters the cells via an active endocytic process facilitated by the ultra-deformable nature of the vesicles, unlike the free dye, which depends solely on passive transport (Sharma et al., 2023). The increased intracellular accumulation observed with the LCZ-UDEs formulation further supports its potential as a robust delivery carrier for enhancing therapeutic outcomes.

The cellular morphology of HaCaT cells, evaluated using phase contrast microscopy to assess structural alterations following 48 h of exposure to various formulations, *viz*, LCZ-SUS, LCZ-UDEs, and blank UDEs at a concentration of 50 μg/mL, is presented in Fig. 7c. As observed in Fig. 7c (B), the cells treated with the pure LCZ-SUS exhibited apparent signs of cytotoxicity, including disrupted morphology, membrane blebbing, and detachment from the culture surface, along with a notable decrease in cell density in contrast to the control. However, the cells treated with the blank UDEs formulation (Fig. 7c (C)) and the LCZ-UDEs formulation (Fig. 7c (D)) maintained normal cell architecture and confluency, which was quite comparable to that of untreated cells (Fig. 7c (A).

These results provide strong evidence that the LCZ-UDEs formulation is biocompatible, causing no evident cytotoxic effects on the HaCaT cells, thus ratifying the safety potential and patient compliance of the developed formulation (Sharma et al., 2023).

3.14. In vivo skin irritation and safety evaluation

Table S9 outlines the histopathological studies conducted on the animals, which revealed that the LCZ-UDEs gel formulation exhibited no erythema on the skin, in contrast to the MKT-LF cream, which, when applied to animal skin, showed significant redness. As depicted in Fig. 8, the histopathological microphotographs of untreated skin, treated with MKT-LF cream, and LCZ-UDEs gel formulation demonstrated the biocompatibility of the developed LCZ-UDEs gel formulation on the skin, as no marked changes in the histopathology were observed. However, some signs of edema and dermal degeneration were observed in the skin sections of animals receiving once-daily topical applications of MKT-LF cream. The microscopical observation specified that the marketed product disordered the originality of normal skin tissue, whereas the developed LCZ-UDEs gel formulation was found to be skin-compliant in nature. Therefore, this demonstrates that lipoidal carrier systems are compatible with the skin and are safe for external application. The absence of erythema or dermal disruption even at mildly elevated local pH suggests that the LCZ-UDEs gel remains well tolerated under infected skin conditions (Martinez-Rossi et al., 2021).

4. Conclusion

This study successfully establishes a Quality-by-Design optimized UDEs gel as a promising nanocarrier for the topical delivery of LCZ, exhibiting superior vesicle deformability, high drug entrapment, sustained release, and markedly enhanced antifungal efficacy over conventional formulation. The optimized system achieved significantly improved skin permeation, elevated cutaneous drug retention, prolonged epidermal residence, and rapid fungicidal action against *Trichophyton rubrum*, while demonstrating excellent biocompatibility, non-irritancy, and favorable rheological properties. Nonetheless, the limitations remain in terms of long-term stability, scale-up feasibility, and the absence of clinical data. Future research should aim to validate the therapeutic outcomes in human subjects, investigate broader antifungal applications, and explore the potential of this technology for delivering other poorly soluble dermatological agents.

Funding statement

This research was financially supported by Ipca Laboratories, Mumbai, India and the Commonwealth Scholarship Commission, London, UK, through a Commonwealth Split-site Scholarship (Reference: INCN-2023-209), facilitating research work at the University of Lancashire, United Kingdom.

CRediT authorship contribution statement

Akanksha Mahajan: Writing – review & editing, Writing – original draft, Visualization, Validation, Methodology, Investigation, Formal analysis, Data curation, Conceptualization. **Gajanand Sharma:**

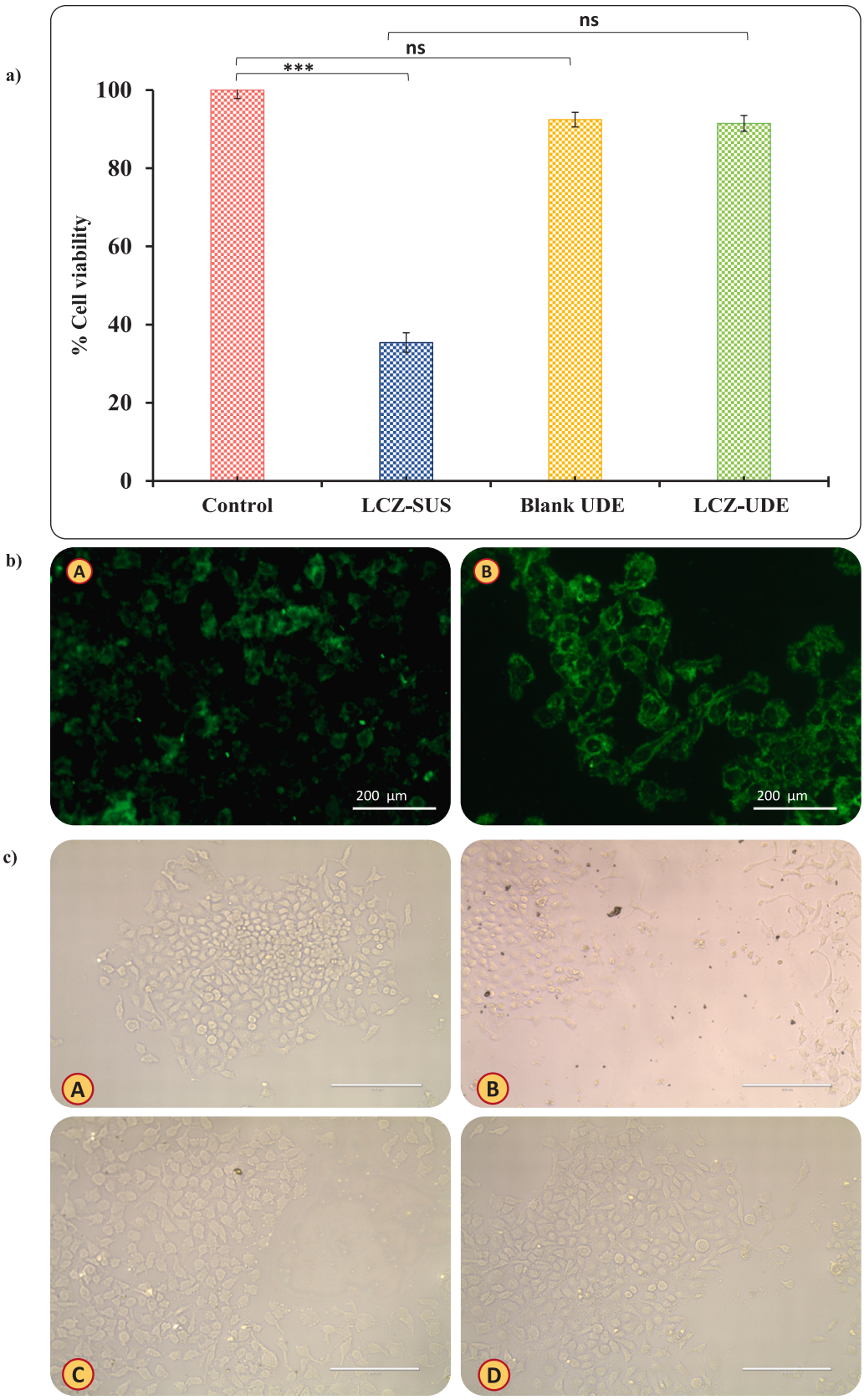

Fig. 7. (a) HaCaT cell viability after 48 h treatment with LCZ-SUS, blank UDEs, and LCZ-UDEs (mean ± SD, n = 3; ***p <0.0001 vs. control; ns = not significant). (b) Fluorescence microscopy of HaCaT cells treated with (A) Coumarin-6 alone and (B) Coumarin-6-loaded LCZ-UDEs, showing enhanced cellular uptake (20X). (c) Phase contrast images of HaCaT cells: (A) untreated, (B) LCZ-SUS, (C) blank UDEs, and (D) LCZ-UDEs, indicating improved cell compatibility (10X/40X).

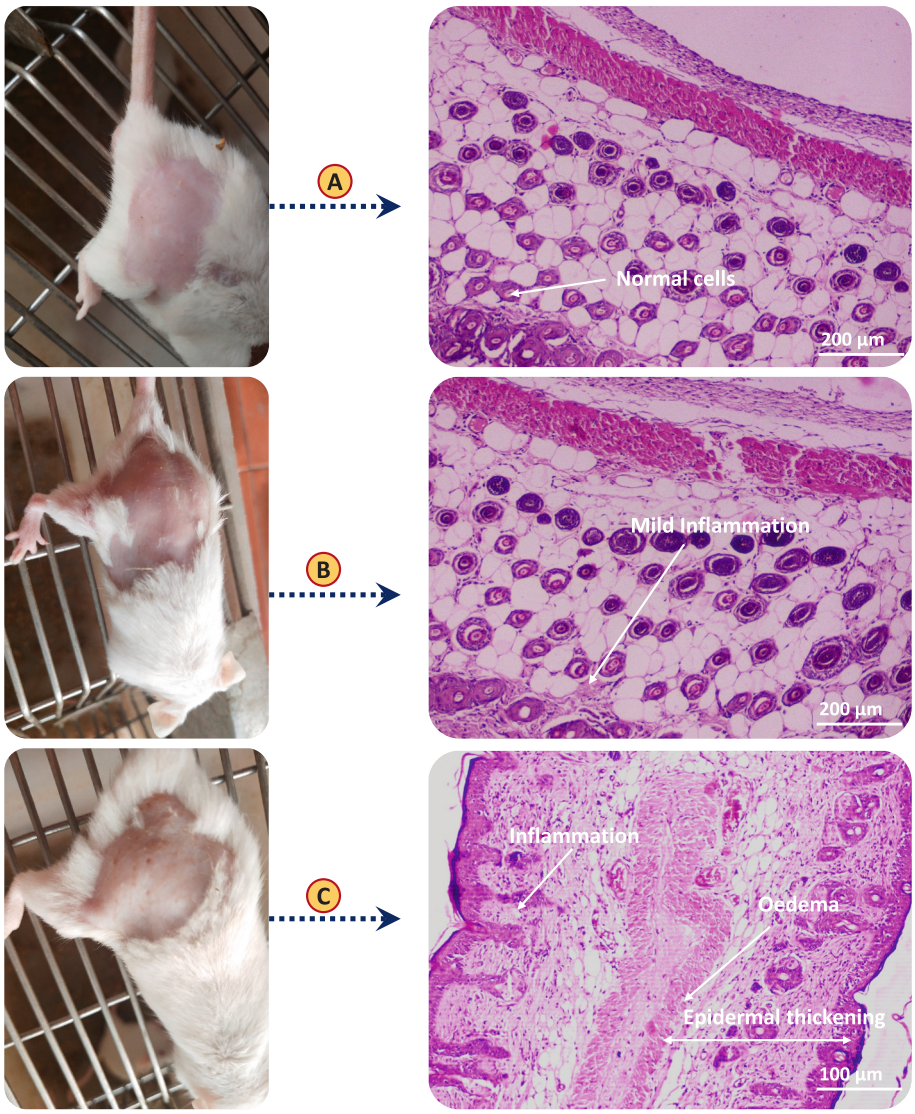

Fig. 8. Photographs of the animal groups showing visible signs of skin inflammation, together with histopathological images of mouse skin: (A) Normal, untreated skin; (B) Skin treated with LCZ-UDEs gel; and (C) Skin treated with MKT-LF cream.

Software, Methodology, Investigation, Formal analysis, Data curation. **Sarah R. Dennison:** Methodology, Validation. **Kamalinder K. Singh:** Writing – review & editing, Supervision, Resources, Funding acquisition, Formal analysis. **Bhupinder Singh:** Writing – review & editing, Validation, Supervision, Software, Methodology, Investigation, Data curation, Conceptualization. **Om Prakash Katare:** Conceptualization, Formal analysis, Funding acquisition, Project administration, Resources, Validation, Writing – review & editing, Supervision.

Declaration of competing interest

The authors declare that they have no known competing financial interests or personal relationships that could have appeared to influence the work reported in this paper.

Acknowledgements

A.M. acknowledges Ipca laboratories, Mumbai, India, for financial assistance as an Industrial Research Fellow. The authors also extend their profound appreciation to the Commonwealth Scholarship Commission, London, UK, for granting financial assistance to the first author (A.M.) as a Commonwealth split-site scholar, enabling the successful execution of microbiology studies conducted at the University of Lancashire, UK. The magnanimity of Stat-Ease Inc., MN, USA, in bestowing perpetual and unlimited access to the licensed version of the Design Expert® software to one of us (B.S.) is also profoundly acknowledged, recognizing his stellar contributions in employing QbD framework to the systematic development of innovative drug delivery systems.

Appendix A. Supplementary data

Supplementary data to this article can be found online at https://doi.org/10.1016/j.ijpharm.2025.126514.

Data availability

All data have been included in the article and supplementary material for the research described in the article.

References

Abdulbaqi, I.M., Darwis, Y., Khan, N.A.K., Assi, R.A., Khan, A.A., 2016. Ethosomal nanocarriers: the impact of constituents and formulation techniques on ethosomal properties, in vivo studies, and clinical trials. Int. J. Nanomed. 11, 2279–2304.

Ahmed, M.G., Biju, P., Shenoy, M.M., Shafeeh, A.R., Mustafa, M., Kanekar, S., Fathima, Z., 2025. Navigating effective therapeutic strategies for dermatophytosis. J. Young Pharm. 17, 7.
Ahuja, N., Katare, O.P., Singh, B., 2007. Studies on dissolution enhancement and mathematical modeling of drug release of a poorly water-soluble drug using water-soluble carriers. Eur. J. Pharm. Biopharm. 65, 26–38.
Al-Smadi, K., Ali, M., Zhu, J., Abdoh, A., Phan, K., Mohammed, Y., 2025. Advances in Characterization of Transdermal and Topical Products using Texture Analyzer Systems. AAPS PharmSciTech. 26, 157.
Alhakamy, N.A., Md, S., Alam, M.S., Shaik, R.A., Ahmad, J., Ahmad, A., Kutbi, H.I., Noor, A.O., Bagalagel, A., Bannan, D.F., 2021. Development, optimization, and evaluation of luliconazole nanoemulgel for the treatment of fungal infection. J. Chem. 2021, 4942659.
Alshetaili, A.S., Almohizea, S., Anwer, M.K., Riadi, Y., 2025. Novel embelin-loaded transniosomes for topical delivery: comprehensive exploration of in vitro, ex vivo and dermatokinetic assessment for anti-cancer activity. J. Sci. Food Agric. 105, 315–328.
Ansari, S.A., Qadir, A., Warsi, M.H., Mujeeb, M., Aqil, M., Mir, S.R., Sharma, S., 2021. Ethosomes-based gel formulation of karanjin for treatment of acne vulgaris: in vitro investigations and preclinical assessment. 3 Biotech 11, 456.
Ashraf, S., Chaudhry, U., Raza, A., Ghosh, D., Zhao, X., 2018. In vitro activity of ivermectin against Staphylococcus aureus clinical isolates. Antimicrob. Resist. Infect. Control 7, 27.
Baghel, S., Nair, V.S., Pirani, A., Sravani, A.B., Bhemisetty, B., Ananthamurthy, K., Aranjani, J.M., Lewis, S.A., 2020. Luliconazole-loaded nanostructured lipid carriers for topical treatment of superficial Tinea infections. Dermatol. Ther. 33, e13959.
Bhargav, E., Reddy, Y.P., Koteshwara, K.B., 2021. Development and optimization of luliconazole nanostructured lipid carriers based gel by quality by design its skin distribution studies, dermatokinetic modeling & in-vitro and ex-vivo correlation. Curr. Drug Deliv. 18, 1041–1053.
Bnyan, R., Khan, I., Ehtezazi, T., Saleem, I., Gordon, S., O'Neill, F., Roberts, M., 2018. Surfactant effects on lipid-based vesicles properties. J. Pharm. Sci. 107, 1237–1246.
Cataldi, S., Ceccarini, M.R., Patria, F., Beccari, T., Mandarano, M., Ferri, I., Lazzarini, A., Curcio, F., Albi, E., 2022. The effect of vitamin D3 and silver nanoparticles on HaCaT cell viability. Int. J. Mol. 23, 1410.
Cevc, G., Vierl, U., 2010. Nanotechnology and the transdermal route: a state of the art review and critical appraisal. J. Control. Release 141, 277–299.
Chalikwar, S.S., Mitkari, P., Patil, K.D., Hatware, K.V., Shete, M.B., 2025. Design of experiments-based optimization of rutin-loaded nanostructured lipid carriers: characterization, pharmacokinetics, and stability evaluation. J. Dispers. Sci. Technol. 1–16.
Chauhan, M., Chandra, J., Gupta, G., Ramaiah, R., Hani, U., Kesharwani, P., 2025. Harnessing phytoconstituents in ethosomes: a new frontier in skin disorder management. Int. J. Pharm. 671, 125273.
Chouhan, S.S., Farooqui, N., Mishra, D.K., 2021. Formulation and evaluation of liposomal loaded nail lacquer containing luliconazole an antifungal drug. Asian J. Pharm. Pharmacol. 7, 131–137.
Dandagi, P.M., Pandey, P., Gadad, A.P., Mastiholimath, V.S., 2020. Formulation and evaluation of microemulsion based luliconazole gel for topical delivery. Indian J. Pharm. Educ. Res 54, 293–301.
Dash, S., Murthy, P.N., Nath, L., Chowdhury, P., 2010. Kinetic modeling on drug release from controlled drug delivery systems. Acta Pol. Pharm. 67, 217–223.
Dave, V., Bhardwaj, N., Gupta, N., Tak, K., 2020. Herbal ethosomal gel containing luliconazole for productive relevance in the field of biomedicine. 3 Biotech 10, 97.
Dellièree, S., Jabet, A., Abdolrasouli, A., 2024. Current and emerging issues in dermatophyte infections. PLoS Pathog. 20, e1012258.
dos Santos Porto, D., Bajerski, L., Donadel Malesuik, M., Soldateli Paim, C., 2022. A review of characteristics, properties, application of nanocarriers and analytical methods of luliconazole. Crit. Rev. Anal. Chem. 52, 1930–1937.
Ebrahimi Barogh, R., Rahimnia, S.M., Nosratabadi, M., Maleki, A., Khosravi Ebrahimi, F., Yahyazade, Z., Haghani, I., Ebrahimnejad, P., Saeedi, M., Armstrong-James, D., 2025. Antifungal efficacy of luliconazole-loaded nanostructured lipid-carrier gel in an animal model of dermatophytosis. J. Fungi 11, 324.
El Maghraby, G.M., Barry, B.W., Williams, A.C., 2008. Liposomes and skin: from drug delivery to model membranes. Eur. J. Pharm. Sci. 34, 203–222.
Erkut, T.S., Coşkun, S., Gümüşderelioğlu, M., 2025. Methylcobalamin-loaded ultra-flexible liposomes: a nanocarrier approach for modulating melanocyte homeostasis and addressing pigmentation imbalances. Int. J. Pharm. 682, 125938.
Espinel-Ingroff, A., Chaturvedi, V., Fothergill, A., Rinaldi, M.G., 2002. Optimal testing conditions for determining mics and minimum fungicidal concentrations of new and established antifungal agents for uncommon molds: NCCLS collaborative study. J. Clin. Microbiol. 40, 3776–3781.
Garg, A.K., Maddiboyina, B., Alqarni, M.H.S., Alam, A., Aldawsari, H.M., Rawat, P., Singh, S., Kesharwani, P., 2021. Solubility enhancement, formulation development and antifungal activity of luliconazole niosomal gel-based system. J. Biomater. Sci. Polym. Ed. 32, 1009–1023.
Garg, V., Singh, H., Bhatia, A., Raza, K., Singh, S.K., Singh, B., Beg, S., 2017. Systematic development of transethosomal gel system of piroxicam: formulation optimization, in vitro evaluation, and ex vivo assessment. AAPS PharmSciTech 18, 58–71. https://doi.org/10.1208/s12249-016-0489-z.
Ghannoum, M.A., Arthington-Skaggs, B., Chaturvedi, V., Espinel-Ingroff, A., Pfaller, M. A., Rennie, R., Rinaldi, M.G., Walsh, T.J., 2006. Interlaboratory study of quality control isolates for a broth microdilution method (modified CLSI M38-A) for testing susceptibilities of dermatophytes to antifungals. J. Clin. Microbiol. 44, 4353–4356.
Gopi, S., Balakrishnan, P., 2024. Revolutionizing transdermal drug delivery: unveiling the potential of cubosomes and ethosomes. J. Mater. Chem. B.
Haider, M., Abdin, S.M., Kamal, L., Orive, G., 2020. Nanostructured lipid carriers for delivery of chemotherapeutics: a review. Pharmaceutics 12, 288.
Hassan, A.S., Hofni, A., Abourehab, M.A.S., Abdel-Rahman, I.A.M., 2023. Ginger extract–loaded transethosomes for effective transdermal permeation and anti-inflammation in rat model. Int. J. Nanomed. 1259–1280.
Helal, D.A., Osama, A., El-Nabarawi, M.A., Teaima, M.H., Ibrahim Al-Samadi, I.E., 2025. Dual-action of clotrimazole loaded − nanosponges vaginal gel for spermicidal action and treatment of vaginal candidiasis: optimization, in-vitro, ex-vivo, and in-vivo experiments. Int. J. Pharm. 670, 125193. https://doi.org/10.1016/j.ijpharm.2025.125193.
Higuchi, T., 1963. Mechanism of sustained-action medication. theoretical analysis of rate of release of solid drugs dispersed in solid matrices. J. Pharm. Sci. 52, 1145–1149. https://doi.org/10.1002/jps.2600521210.
Houacine, C., Adams, D., Singh, K.K., 2020. Impact of liquid lipid on development and stability of trimyristin nanostructured lipid carriers for oral delivery of resveratrol. Journal of Molecular Liquids 316, 113734.
Hussain, A., Altamimi, M.A., Afzal, O., Altamimi, A.S.A., Ramzan, M., Khuroo, T., 2023. Mechanistic of vesicular ethosomes and elastic liposomes on permeation profiles of acyclovir across artificial membrane, human cultured epiderm, and rat skin: in vitro-ex vivo study. Pharmaceutics. https://doi.org/10.3390/pharmaceutics15092189.
Kapileshwari, G.R., Barve, A.R., Kumar, L., Bhide, P.J., Joshi, M., Shirodkar, R.K., 2020. Novel drug delivery system of luliconazole - Formulation and characterisation. J. Drug Deliv. Sci. Technol. 55, 101302. https://doi.org/10.1016/j.jddst.2019.101302.
Kaur, A., Bhoop, B.S., Chhibber, S., Sharma, G., Gondil, V.S., Katare, O.P., 2017. Supramolecular nano-engineered lipidic carriers based on diflunisal-phospholipid complex for transdermal delivery: QbD based optimization, characterization and preclinical investigations for management of rheumatoid arthritis. Int. J. Pharm. 533, 206–224. https://doi.org/10.1016/j.ijpharm.2017.09.041.
Kaur, M., Singh, G., Shivgotra, R., Singh, M., Thakur, S., Jain, S.K., 2024. Prolonged skin retention of luliconazole from SLNs based topical gel formulation contributing to ameliorated antifungal activity. AAPS PharmSciTech 25, 229.
Kaur, M., Singh, K., Jain, S.K., 2020. Luliconazole vesicular based gel formulations for its enhanced topical delivery. J. Liposome Res. 30, 388–406.
Khan, I., Needham, R., Yousaf, S., Houacine, C., Islam, Y., Bnyan, R., Sadozai, S., Elrayess, M., Elhissi, A., 2021. Impact of phospholipids, surfactants and cholesterol selection on the performance of transfersomes vesicles using medical nebulizers for pulmonary drug delivery. J. Drug Deliv. Sci. Technol. https://doi.org/10.1016/j.jddst.2021.102822.
Kumar, M., Shanthi, N., Mahato, A.K., Soni, S., Rajnikanth, P.S., 2019. Preparation of luliconazole nanocrystals loaded hydrogel for improvement of dissolution and antifungal activity. Heliyon 5.
Kumar, P., Ramachandran, S., Das, S., Bhattacharya, S.N., Taneja, B., 2023. Insights into changing dermatophyte spectrum in india through analysis of cumulative 161,245 cases between 1939 and 2021. Mycopathologia 188, 183–202. https://doi.org/10.1007/s11046-023-00720-6.
Kumar, V., Ain, S., Kumar, B., Ain, Q., 2020. Optimization and evaluation of topical gel containing solid lipid nanoparticles loaded with luliconazole and its anti-fungal activity. Int. J. Pharm. Res.
Kuo, S.H., Shen, C.J., Shen, C.F., Cheng, C.M., 2020. Role of pH value in clinically relevant diagnosis. Diagnostics 10, 107.
Lan, Y., Wang, J., Li, H., Zhang, Y., Chen, Y., Zhao, B., Wu, Q., 2016. Effect of menthone and related compounds on skin permeation of drugs with different lipophilicity and molecular organization of stratum corneum lipids. Pharm. Dev. Technol. 21, 389–398.
Limongi, T., Susa, F., Marini, M., Allione, M., Torre, B., Pisano, R., di Fabrizio, E., 2021. Lipid-Based Nanovesicular Drug Delivery Systems. Nanomater. (Basel, Switzerland) 11. https://doi.org/10.3390/nano11123391.
Lin, B., Wang, W., Ba, W., Li, H., Fan, J., 2022. Preparation and partial pharmacodynamic studies of luliconazole ethosomes. Clin. Exp. Pharmacol. Physiol. 49, 549–557.
Liu, R.J., Li, M., Zhu, Q., Liu, H.Y., Zhang, X.X., Han, X.Y., Yu, M.J., Zhou, J.W., Han, C. Y., 2025. Development and characterization of a hydrogel containing chloramphenicol-loaded binary ethosomes for effective transdermal permeation and treatment acne in rat model. Int. J. Nanomedicine 1697–1715.
Madawi, E.A., Al Jayoush, A.R., Rawas-Qalaji, M., Thu, H.E., Khan, S., Sohail, M., Mahmood, A., Hussain, Z., 2023. Polymeric nanoparticles as tunable nanocarriers for targeted delivery of drugs to skin tissues for treatment of topical skin diseases. Pharmaceutics 15, 657.
Maeda, J., Nanjoh, Y., Koga, H., Toga, T., Makimura, K., Tsuboi, R., 2016. In vitro antifungal activity of luliconazole against trichophyton spp. Med. Mycol. J. 57, J1–J6. https://doi.org/10.3314/mmj.57.J1.
Mahmood, A., Rapalli, V.K., Gorantla, S., Waghule, T., Singhvi, G., 2022. Dermatokinetic assessment of luliconazole-loaded nanostructured lipid carriers (NLCs) for topical delivery: QbD-driven design, optimization, and in vitro and ex vivo evaluations. Drug Deliv. Transl. Res. 12, 1118–1135.
Makwana, H., Joshi, D., Kulkarni, M., Shah, S., Acharya, S., 2025. Comparative evaluation of clove oil and tea tree oil based topical microemulsion gel in modulating delivery of luliconazole through skin: promising approach for antifungal delivery. J. Dispers. Sci. Technol. 1–17.
Mall, J., Naseem, N., Haider, M.F., Rahman, M.A., Khan, S., Siddiqui, S.N., 2024. Nanostructured lipid carriers as a drug delivery system: a comprehensive review with therapeutic applications. Intell. Pharm.
Manconi, M., Caddeo, C., Nacher, A., Diez-Sales, O., Peris, J.E., Ferrer, E.E., Fadda, A.M., Manca, M.L., 2019. Eco-scalable baicalin loaded vesicles developed by combining

phospholipid with ethanol, glycerol, and propylene glycol to enhance skin permeation and protection. Colloid. Surf. B Biointerf. 184, 110504.
Martinez-Rossi, N.M., Peres, N.T.A., Bitencourt, T.A., Martins, M.P., Rossi, A., 2021. State-of-the-art dermatophyte infections: epidemiology aspects, pathophysiology, and resistance mechanisms. J. Fungi. https://doi.org/10.3390/jof7080629.
Marto, J., Vitor, C., Guerreiro, A., Severino, C., Eleutério, C., Ascenso, A., Simões, S., 2016. Ethosomes for enhanced skin delivery of griseofulvin. Colloid. Surf. B Biointerf. 146, 616–623. https://doi.org/10.1016/j.colsurfb.2016.07.021.
Mehmood, Y., Shahid, H., Ahmed, S., Khursheed, A., Jamshaid, T., Jamshaid, M., Mengistie, A.A., Dawoud, T.M., Siddique, F., 2024. Synthesis of vitamin D3 loaded ethosomes gel to cure chronic immune-mediated inflammatory skin disease: physical characterization, in vitro and ex vivo studies. Sci. Rep. 14, 23866. https://doi.org/10.1038/s41598-024-72951-6.
Molinaro, R., Gagliardi, A., Mancuso, A., Cosco, D., Soliman, M.E., Casettari, L., Paolino, D., 2019. Development and in vivo evaluation of multidrug ultradeformable vesicles for the treatment of skin inflammation. Pharmaceutics 11, 644.
Mukherjee, P.K., Leidich, S.D., Isham, N., Leitner, I., Ryder, N.S., Ghannoum, M.A., 2003. Clinical Trichophyton rubrum strain exhibiting primary resistance to terbinafine. Antimicrob. Agents Chemother. 47, 82–86.
Natsheh, H., Touitou, E., 2020. Phospholipid vesicles for dermal/transdermal and nasal administration of active molecules: the effect of surfactants and alcohols on the fluidity of their lipid bilayers and penetration enhancement properties. Molecules 25, 2959.
Nene, S., Shah, S., Rangaraj, N., Mehra, N.K., Singh, P.K., Srivastava, S., 2021. Lipid based nanocarriers: a novel paradigm for topical antifungal therapy. J. Drug Deliv. Sci. Technol. 62, 102397.
Nidbane, A., Dound, A., Satpute, K., Syed, S.M., 2025. Development of a novel luliconazole transferosomal gel for enhanced antifungal delivery. J. Dermatol. Sci. Cosmet. Technol. 2, 100071.
Nirbhavane, P., Sharma, G., Singh, B., Khuller, G.K., Goni, V.G., Patil, A.B., Katare, O.P., 2018. Preclinical Explorative Assessment of Celecoxib-Based Biocompatible Lipidic Nanocarriers for the Management of CFA-Induced Rheumatoid Arthritis in Wistar Rats. AAPS PharmSciTech 19, 3187–3198.
Niu, J., Yuan, M., Li, H., Liu, Y., Wang, L., Fan, Y., Zhang, Y., Liu, X., Li, L., Zhang, J., 2022. Pentapeptide modified ethosomes for enhanced skin retention and topical efficacy activity of indomethacin. Drug Deliv. 29, 1800–1810.
Noreen, S., Ehsan, S., Ghumman, S.A., Hasan, S., Batool, F., Ijaz, B., Shirinfar, B., Alsader, K.A.M., Ahmed, N., 2023. Polymeric complex nanocarriers of Mangifera indica gum & chitosan for methotrexate delivery: formulation, characterization, and in vitro toxicological assessment. J. Drug Deliv. Sci. Technol. 88, 105001.
Nosratabadi, M., Rahimnia, S.M., Barogh, R.E., Abastabar, M., Haghani, I., Akhtari, J., Hajheydari, Z., Ebrahimnejad, P., 2024. Luliconazole-loaded nanostructured lipid carrier: formulation, characterization, and in vitro antifungal evaluation against a panel of resistant fungal strains. Sci. Rep. 14, 30708.
Pant, A., Sharma, G., Saini, S., Kaur, G., Jain, A., Thakur, A., Singh, B., 2024a. QbD-driven development of phospholipid-embedded lipidic nanocarriers of raloxifene: extensive in vitro and in vivo evaluation studies. Drug Deliv. Transl. Res. 14, 730–756.
Pant, A., Singh, G., Barnwal, R.P., Sharma, T., Singh, B., 2024b. QbD-driven development and characterization of superparamagnetic iron oxide nanoparticles (SPIONS) of a bone-targeting peptide for early detection of osteoporosis. Int. J. Pharm. 654, 123936.
Panthi, V.K., Nepal, U., 2022. Formulation and Development of a Water-in-Oil Emulsion-Based Luliconazole Cream: In Vitro Characterization and Analytical Method Validation by RP-HPLC. Int. J. Anal. Chem. 2022, 7273840.
Peram, M.R., Patil, S.R., Suryadevara, V., Yarguntla, S.R., Kamalakar, S., Patil, P., Paravastu, K.K., Kugaji, M., Nadaf, S., 2025. Phospholipid-Based Ultraflexible Nanovesicular Gel of Sertaconazole Nitrate for the Treatment of Skin Fungal Infections: Statistical Optimization, In Vitro and Preclinical Assessment. Gels 11, 909.
Pinilla, C.M.B., Lopes, N.A., Brandelli, A., 2021. Lipid-based nanostructures for the delivery of natural antimicrobials. Molecules 26, 3587.
Pople, P.V., Singh, K.K., 2011. Development and evaluation of colloidal modified nanolipid carrier: Application to topical delivery of tacrolimus. European Journal of Pharmaceutics and Biopharmaceutics 79 (1), 82–94.
Prajapati, S.K., Jain, A., Bajpai, M., 2025. Lipid-based nanoformulations in onychomycosis therapy: addressing challenges of current therapies and advancing treatment. RSC Adv. 15, 7799–7825.
Sæbø, I., Bjørås, M., Franzyk, H., Helgesen, E., Booth, J., 2023. Optimization of the hemolysis assay for the assessment of cytotoxicity. Int. J. Mol. Sci. 24, 2914.
Saini, K., Modgill, N., Singh, K.K., Kakkar, V., 2022. Tetrahydrocurcumin lipid nanoparticle based gel promotes penetration into deeper skin layers and alleviates atopic Dermatitis in 2,4-Dinitrochlorobenzene (DNCB) mouse model. Nanomater. (Basel) 12, 636.
Santos, D.A., Hamdan, J.S., 2005. Evaluation of broth microdilution antifungal susceptibility testing conditions for Trichophyton rubrum. J. Clin. Microbiol. 43, 1917–1920.
Saroj, S., Saha, S., Ali, A., Gupta, S.K., Bharadwaj, A., Agrawal, T., Pal, S., Rakshit, T., 2024. Plant extracellular nanovesicle-loaded hydrogel for topical antibacterial wound healing in vivo. ACS Appl. Bio Mater. 8, 1–11.
Sarolia, J., Baldha, R., Chakraborthy, G., Rathod, S., 2023. The effect of edge activator on the evolution and application of a nonionic surfactant: the elastic vesicular system. J. Surfactant Deterg. 26, 747–759.
Seenivasan, R., Halagali, P., Nayak, D., Tippavajhala, V.K., 2025. Transethosomes: a comprehensive review of ultra-deformable vesicular systems for enhanced transdermal drug delivery. AAPS PharmSciTech. 26, 41.
Shah, N., Prajapati, R., Gohil, D., Aundhia, C., Sadhu, P., Kardani, S., 2023. Luliconazole loaded niosomal topical gel: factorial design, in vitro characterization and antifungal study. Indian J. Pharm. Educ. Res. 57, s520–s527.
Shaikh, M.S., Kale, M.A., Shaikh, M.D.M., Mahaparale, P.R., 2022. Formulation, characterization and antimicrobial studies of lyophilized luliconazole nanosuspension for enhancing solubility using modified polymer. Int. J. Polym. Mater. Polym. Biomater. 71, 692–706.
Sharma, G., Devi, N., Thakur, K., Jain, A., Katare, O.P., 2018. Lanolin-based organogel of salicylic acid: evidences of better dermatokinetic profile in imiquimod-induced keratolytic therapy in BALB/c mice model. Drug Deliv. Transl. Res. 8, 398–413.
Sharma, G., Kaur, B., Thakur, K., Mahajan, A., Amarji, B., Singh, M.P., Katare, O.P., 2022. Pluronic F127-tailored lecithin organogel of acyclovir: Preclinical evidence of antiviral activity using BALB/c murine model of cutaneous HSV-1 infection. Drug Deliv. Transl. Res. 12, 213–228.
Sharma, G., Mahajan, A., Nirbhavane, P., Singh, G., Barnwal, R.P., Singh, B., Katare, O. P., 2025a. Evaluating in-depth potential of Pluronic F127-tailored complex micellar systems of etodolac for the therapeutic management of uveitis: A comprehensive preclinical study. Int J Pharm 687, 126390.
Sharma, G., Mahajan, A., Thakur, K., Kaur, G., Goni, V.G., Kumar, M.V., Barnwal, R.P., Singh, G., Singh, B., Katare, O.P., 2023. Exploring the therapeutic potential of sodium deoxycholate tailored deformable-emulsomes of etodolac for effective management of arthritis. Sci. Rep. 13, 21681.
Sharma, G., Thakur, A., Singh, J., Kaur, G., Singh, B., Raza, K., Katare, O.P., 2025b. Investigating in-depth potential of lipid-engineered emulsomes of aceclofenac for the management of arthritis: a comprehensive preclinical study. Inorg. Chem. Commun. 172, 113737.
Sharma, G., Thakur, A., Singh, V., Thakur, K., Nirbhavane, P., Raza, K., Katare, O.P., 2024. Strategic development of aceclofenac loaded organosomes for topical application: an explorative ex-vivo and in-vivo investigation for arthritis. Int. J. Pharm. 666, 124762.
Sharma, G., Yukhti, Y., Kanika, T., Akanksha, M., Gurjeet, K., Bhupinder, S., Kaisar, R., Katare, O.P., 2021. Co-delivery of isotretinoin and clindamycin by phospholipid-based mixed micellar system confers synergistic effect for treatment of acne vulgaris. Exp. Opin. Drug Deliv. 18, 1291–1308.
Song, H., Wen, J., Li, H., Meng, Y., Zhang, Y., Zhang, N., Zheng, W., 2019. Enhanced transdermal permeability and drug deposition of rheumatoid arthritis via sinomenine hydrochloride-loaded antioxidant surface transethosome. Int. J. Nanomed. 3177–3188.
Souto, E.B., Macedo, A.S., Dias-Ferreira, J., Cano, A., Zielińska, A., Matos, C.M., 2021. Elastic and ultradeformable liposomes for transdermal delivery of Active Pharmaceutical Ingredients (APIs). Int. J. Mol. Sci. 22, 9743.
Thakur, K., Mahajan, A., Sharma, G., Singh, B., Raza, K., Chhibber, S., Katare, O.P., 2020. Implementation of Quality by Design (QbD) approach in development of silver sulphadiazine loaded egg oil organogel: an improved dermatokinetic profile and therapeutic efficacy in burn wounds. Int. J. Pharm. 576, 118977.
Thakur, K., Sharma, G., Singh, B., Chhibber, S., Katare, O.P., 2019. Nano-engineered lipid-polymer hybrid nanoparticles of fusidic acid: an investigative study on dermatokinetics profile and MRSA-infected burn wound model. Drug Deliv. Transl. Res. 9, 748–763.
Thakur, K., Sharma, G., Singh, B., Chhibber, S., Patil, A.B., Katare, O.P., 2018. Chitosan-tailored lipidic nanoconstructs of Fusidic acid as promising vehicle for wound infections: an explorative study. Int. J. Biol. Macromol. 115, 1012–1025.
Thiramanas, R., Wongngam, Y., Supanakorn, G., Polpanich, D., 2024. BSA adsorption on titanium dioxide nanoparticle surfaces for controlling their cellular uptake in skin cells. ACS Appl. Bio Mater. 7, 1713–1722.
Touitou, E., Dayan, N., Bergelson, L., Godin, B., Eliaz, M., 2000. Ethosomes-novel vesicular carriers for enhanced delivery: characterization and skin penetration properties. J. Control. Release 65, 403–418.
Touitou, E., Natsheh, H., 2024. The evolution of emerging nanovesicle technologies for enhanced delivery of molecules into and across the skin. Pharmaceutics 16, 267.
Vats, A., Nigam, P., 2023. Fluconazole and luliconazole nanoemulsion: a comprehensive study on synergistic efficacy, pharmacokinetics, and novel applications in antifungal therapy. PEXACY Int. J. Pharm. Sci. 2, 1–19.
Waghule, T., Shalini, P., Vamshi Krishna, R., Vishal, G., Srividya, G., Sunil, K.D., Ranendra Narayan, S., Singhvi, G., 2021. Improved skin-permeated diclofenac-loaded lyotropic liquid crystal nanoparticles: QbD-driven industrial feasible process and assessment of skin deposition. Liq. Cryst. 48, 991–1009.
Wiederhold, N., Mccarthy, D., Tavakkol, A., 2014. Luliconazole demonstrates potent in vitro activity against dermatophytes recovered from patients with onychomycosis. Antimicrob. Agents Chemother. 58, 3553–3555.
Yang, Z., Wang, Q., Ma, K., Shi, P., Liu, W., Huang, Z., 2018. Fluconazole inhibits cellular ergosterol synthesis to confer synergism with berberine against yeast cells. J. Glob. Antimicrob. Resist. 13, 125–130.
Yılmaz Usta, D., Teksin, Z.S., Tugcu-Demiroz, F., 2024. Evaluation of emulgel and nanostructured lipid carrier-based gel formulations for transdermal administration of ibuprofen: characterization, mechanical properties, and ex-vivo skin permeation. AAPS PharmSciTech 25, 124.
Zhan, B., Wang, J., Li, H., Xiao, K., Fang, X., Shi, Y., Jia, Y., 2024. Ethosomes: a promising drug delivery platform for transdermal application. Chemistry (Easton). 6, 993–1019.